Petroleum Science 20 (2023) 1395–1410

Contents lists available at ScienceDirect

Petroleum Science

journal homepage: www.keaipublishing.com/en/journals/petroleum-science

Original Paper

The control of astronomical cycles on lacustrine fine-grained event Sedimentation—A case study of the Chunshang sub-member of the upper Es_4 in the Dongying Sag

Tian-Yu Xu [a, b], Jun Peng [a, b, *], Le-Dan Yu [a, b], Hao-Dong Han [c], Yi-Ming Yang [a, b], Yao Zeng [a, b], Yu-Bin Wang [a, b]

[a] School of Geoscience and Technology, Southwest Petroleum University, Chengdu, Sichuan, 610500, China
[b] Natural Gas Geology Key Laboratory of Sichuan Province, Sothwest Petroleum University, Chengdu, Sichuan, 610500, China
[c] Chengdu Geological Survey Center, China Geological Survey, Chengdu, Sichuan, 610081, China

ARTICLE INFO

Article history:
Received 8 February 2022
Received in revised form
11 October 2022
Accepted 29 November 2022
Available online 5 December 2022

Edited by Jie Hao and Teng Zhu

Keywords:
Astronomical cycle
Fine-grained event sedimentation
Long eccentricity
Chunshang sub-member of the upper Es_4
Dongying Sag

ABSTRACT

Fine-grained lacustrine sedimentation controlled by astronomical cycles remains a research weakness in sedimentology studies, as most studies have concentrated on how astronomical cycles affect the normal lacustrine fine-grained sedimentation, but how they affect the lacustrine fine-grained event sedimentation has been rarely studied. Therefore, this work researched the characteristics of event sedimentation by systematically observing the cores from 30 cored wells in the Shahejie Formation of the Dongying Sag at a depth of over 1800 m, with more than 4000 thin sections being authenticated and over 1000 whole rocks being analyzed by X-ray diffraction (XRD). The research object was the Chunshang Sub-member of Upper Es_4 in the Fanye 1 well, as it had the most comprehensive analysis data and underwent the most continuous coring. We divided astronomical cycles into different orders and made corresponding curves using the gamma-ray (GR) curve, spectral analysis, power spectrum estimation, and module extreme values, there were 6 long eccentricity periods, 22 short eccentricity periods, 65.5 obliquity cycles, and 110.5 precession cycles in this sub-member. On this basis, this study analyzed the control of astronomical cycles on the lacustrine fine-grained event sedimentation, and the research shows deposits were developed by slide-slump, turbidities, hyperpycnites, and tempestites in the Chunshang Sub-member of the Upper Es_4, with higher long eccentricity, the monsoon climate contributes to the formation of storm currents, while with lower long eccentricity, the surface deposits are severely eroded by rivers and rainfalls, thus developing the slide-slump, turbidities, and hyperpycnites. The relationship between the lacustrine fine-grained event sedimentation and astronomical cycles was studied in this case study, which can promote research on fine-grained sedimentary rocks in genetic dynamics and boost the theoretical and disciplinary development in fine-grained sedimentology.

1. Introduction

With progress made in unconventional oil and gas exploration, the theory of fine-grained sedimentology has developed rapidly, making the genesis of fine-grained sedimentary rocks a research hotspot. Generally, fine-grained sediments are weak hydrodynamic products mostly developed in deep waters via slow and normal sedimentation (Potter et al., 2005). However, a flume experiment verified that fine-grained sediments could be moved and deposited at a specific flow velocity (Schieber et al., 2007), overthrowing the traditional argument that mudstone could only be deposited in still waters. Later, scholars worldwide continuously found various event deposits in fine-grained sedimentary rocks, including wave-enhanced gravity flows deposition (Macquaker et al., 2010), hyperpycnites (Plint, 2014; Wilson and Schieber, 2014; Yang et al., 2015), storm deposits (Plint, 2014; Zhang et al., 2016), slide-slump (Cao et al., 2021), turbidities (Zhang et al., 2016), and debris flows deposition (Yuan et al., 2015). The event sedimentation

* Corresponding author. School of Geoscience and Technology, Southwest Petroleum University, Chengdu, Sichuan, 610500, China.
E-mail address: 15531516085@163.com (J. Peng).

https://doi.org/10.1016/j.petsci.2022.11.023

of fine-grained rocks not only sheds light on the paleoenvironment but also functions as important reservoirs and sweet spot areas for unconventional oil and gas resource exploration. Therefore, theoretically, discussing the forming mechanism of fine-grained event sedimentation helps clarify its major controlling factors and working patterns. Meanwhile, it contributes to understanding the environmental influence of frequent climate changes, which guides predicting future climate conditions. In production, such discussion contributes to studying the cause of high-quality reservoir mechanisms and offers an essential basis for predicting unconventional oil and gas source-reservoir-cap assemblage and favorable reservoir development zone. Research shows that the distribution of event sedimentation is mostly controlled by water depths and climate changes, which are related to astronomical cycles (He et al., 2019; Fu et al., 2020; Xing et al., 2020; Chen et al., 2021a,b). Current geological research on astronomical cycles mainly focuses on fields such as stratigraphy (Mei, 2015; Gao et al., 2020; Liu and Liu, 2020), paleoclimatology (Li et al., 2019; Zhao et al., 2019), and paleontology (Li et al., 2016), while limited studies were conducted on the relationship between astronomical cycles and event sedimentation despite discussion and speculation made by Wang et al., 2015b and Yang and Tian (2020). Thus, to a certain extent, the public has limited knowledge of this issue, which restricts further exploration of event deposits controlling factors and distribution rules, thus impeding the fine-grained sedimentological theory and effective unconventional oil and gas resources exploration.

The Dongying Sag, located in Bohai Bay Basin is rich in oil and gas, and its fine-grained rocks of the Upper Es_4 (the fourth member of the Shahejie Formation) have huge potential for oil and gas exploration. The area is less affected by geological tectonics, and the fine-grained sedimentary rocks are sensitive to climate change, making it suitable for identifying astronomical cycle signals. Previous studies have made certain progress in this regard. For example, Sun et al. (2017) used spectral analysis and wavelet transform methods to identify the Milankovitch cycle in the Dongying Sag. They used core, X-ray diffraction, and geochemical data to delineate eight petrographic types and established a depositional model for fine-grained sedimentary rock facies. Jin (2017) used the GR logging curve of the Fanye 1 well in the Dongying Sag as a proxy for the stratigraphic analysis of the astronomical rotation, revealing that the lithology and variations in lithologic assemblages of the Chunshang Sub-member of the Upper Es_4 corresponded well to the 38 kyr astronomical cycle. Taking into account the exploration practice and by comparing the stratigraphic delineation schemes in the Jiyang Depression, Shi et al. (2019a) used the long eccentricity, short eccentricity and slope period curves as reference curves for the four-, five- and six-stage sequences delineation, thus achieving quantitative high-frequency sequences delineation of lacustrine fine-grained sedimentary rocks. Shi et al. (2019b, 2020) and Luan et al. (2022) restored the paleoclimatic and paleoenvironmental variation characteristics of lake sedimentation in the Dongying Sag from the perspective of astronomical cycle-controlled sedimentation. They also explored the genesis mechanism of lacustrine fine-grained sedimentary rocks, which has both scientific and guiding significance for exploring unconventional oil and gas. Jin et al. (2022) determined the optimal sedimentation rate by fitting the observed sedimentation cycle to the astronomical cycle. They reconstructed the relative lake level variation curve during the deposition period from the Chunshang Sub-member of the Upper Es_4 to the lower Es_3 with a sedimentation noise model based on a 100 kyr orbital tuning. This work observed core and microscope thin-section, and found that this zone is characterized by event sedimentation, including slide-slump, turbidities, hyperpycnites, tempestites, etc. Although many scholars have studied the relations of local strata, lithofacies, paleoenvironment, etc. with astronomical cycles, few studies have investigated how these cycles affect the causes of fine-grained event sedimentation so that the deposition law of fine-grained rocks of the Upper Es_4 remains unclear, which further restricts the exploration of unconventional oil and gas resources.

This study took the Chunshang Sub-member of the Upper Es_4 in the Dongying Sag as an example and researched the fine-grained event sedimentation and its various types by core observation, thin section authentication, XRD of whole rocks, and element geochemistry analysis. On this basis, the Chunshang Sub-member of the Upper Es_4 in the Fanye 1 well was chosen as the research object as it had the most comprehensive analysis data and underwent the most continuous coring. Afterwards, based on the GR curve and the theory of Milankovitch cycles, we carried out the spectral analysis, power spectrum estimation, and module extreme values to categorize astronomical cycles into different orders and to establish astronomical circulars. Then, this study discussed how these cycles controlled the fine-grained event sedimentation by regulating the paleoclimate and paleo-water depth, providing references for their relationship and further developing the theory of fine-grained sedimentology and assisting strata optimization and further oil and gas exploration of fine-grained sediments in the study area.

2. Geological settings

Dongying Sag, a typical Meso-Cenozoic continental rift basin located in the Jiyang Depression of Bohai Bay Basin, is surrounded by the Qingtuozi Heave in the east, the Luxi Uplift and Guangrao Heave in the south, the Qingcheng Heave in the west, and the Chenjiazhuang and Binxian Heaves in the north (Fig. 1). Covering an area of about 5700 km^2, the depression is 90 km long from east to west and 65 km wide from south to north, including three positive tectonic belts (northern steep slope zone, central anticlinal zone, and southern gentle slope zone) and four negative tectonic belts (Lijin, Niuzhuang, Boxing and Minfeng Subsags). As the Paleogene Chunshang Sub-member of the Upper Es_4 was formed in half-deep and deep lakes, the fine-grained sedimentary rocks were well developed, with the major lithology including argillaceous limestone, lime clay rock, lime-containing clay rock, clay rock, and dolomitic clay rock.

3. Experiment and data processing methods

3.1. Core observation and thin-section identification

This study systematically observed about 1800 m cores from 30 cored wells, including Fanye 1, Niuye 1, Guan 17-Xie 10, and Wang 129 wells from the fourth member of Shahejie Formation in Dongying Sag, and identified over 4000 thin sections from the wells.

3.2. X-ray diffraction (XRD) analysis

X-ray diffraction (XRD) analysis was carried out to analyze the content of pyrites and carbonate minerals. Samples were ground into particles less than 300 mesh size, and 1 g powder was put into a sample sink and pressed with ground glass to fill the sink. Afterwards, the sample was placed at the center of a goniometer. All pretreatment, such as grinding and tableting, and analysis, was made by the strata office of Sinopec Shengli Exploration and Production Research Institute via DX-2700B X-ray analyzer under SY/T5163-2010 industry standard for the experiment. Cu and Ka were set as X-rays. The instrument was operated at 40 kV tube voltage and 30 mA tube flow under a 21 °C ambient temperature with a humidity of 40%. The scanning pattern was θ-θ. The contents

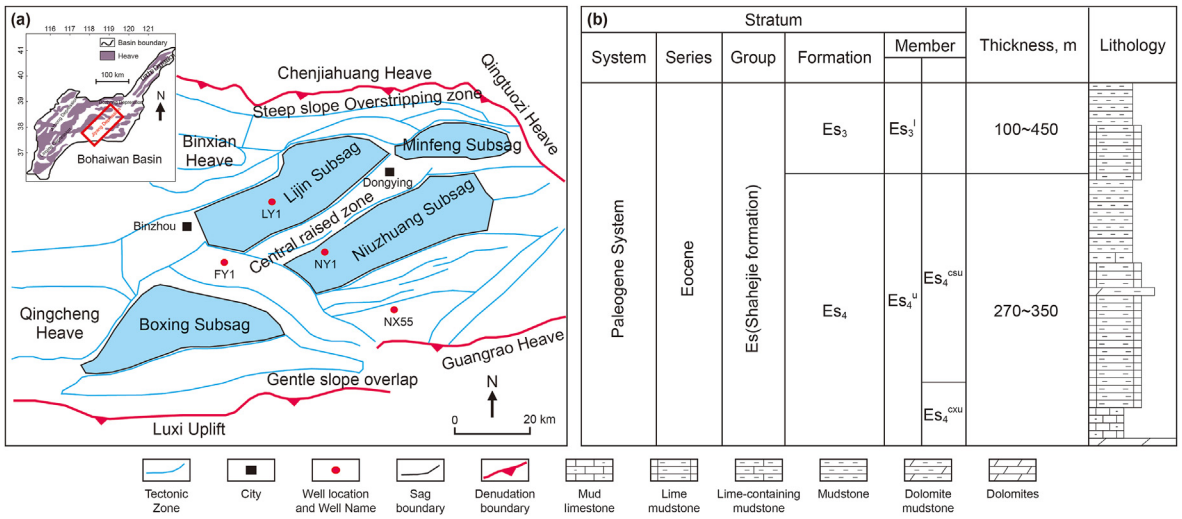

Fig. 1. **(a)** Geologic structure diagram of the Dongying Sag; **(b)** Stratigraphic column for the lithology in the Chunshang Sub-member of the Upper Es_4 (right) (Wu et al., 2017)

of clay minerals, felsic rocks, carbonate minerals, and pyrite in a 300 g sample were measured, and this study focused on the statistics of carbonate minerals and pyrite.

3.3. Element analysis

The Itrax XRF core scanner was adopted to analyze the elements in samples through a Mo tube test to understand their Na and Al contents, which was conducted by the Sinopec Shengli Exploration and Production Research Institute. A 4 μm thin layer of Ultralene was covered on the sample profile to avoid contaminating the equipment and reduce the surface roughness. During the scanning, five points were selected for the test of each sample, and the average value was calculated. Each sample test was conducted for 20 s under 30 kV tube voltage and 30 mA tube flow. 128 m cores were scanned and analyzed, and primary and minor elements data were achieved, including Na, Al, Ca, Ba, Fe, Pb, Ni, Sr, and Ti, among which Na and Al were further studied.

3.4. Organic carbon analysis

LECOCS-230 carbon-sulfur analyzer was employed in the test and analysis according to the GB/T19145—2003 Chinese national standard by the State Key Laboratory of Oil and Gas Reservoir Geology and Exploitation of Southwest Petroleum University. The samples were ground into powders with less than 0.2 mm diameter before diluting hydrochloric acid (1 hydrochloric acid: 7 water for preparation) was used to remove the inorganic carbon component. Afterwards, processed samples were burnt with high-temperature oxygen (99.9% oxygen purity), transforming organic carbon to CO_2. Thus, an infrared spectrum detector could achieve the total organic carbon content. In total, 200 samples were involved in this organic carbon analysis.

3.5. Well-logging data processing methods

Common methods of astronomical cycle research via well-logging data include spectral analysis, wavelet transformation, and power spectrum estimation to extract ground response information about earth orbital parameters, which could help determine the stratigraphic age of the Ma scale (Ikeda and Tada, 2014; Ruhl et al., 2016; Huang, 2019; Ma et al., 2019; DerMeulen et al., 2020; Yu et al., 2021). As Chunshang Sub-member of Upper Es_4 in the Fanye 1 well had the most comprehensive analysis data and underwent the most continuous coring, we processed its gamma-ray logging data.

One-dimension continuous wavelet toolbox provided by Matlab was used to reduce signal disturbance and avoid non-continuous stratigraphic records, guaranteeing the credibility of research results. We then used Past3.0 statistical analysis software containing various mainstream spectral analysis methods and its REDFIT software pack to analyze the pretreated gamma-ray logging data. Compared with other counterparts, REDFIT was characterized by its convenient application without interpolation. With the assistance of the one-dimension continuous wavelet toolbox, the Morlet wavelet was selected for a one-dimension continuous wavelet transform of gamma-ray well-logging data signals, which generated more reliable results as it provided a statistically significant test. Based on wavelet analysis, a coefficient matrix could be achieved to calculate extreme modulus values. While searching for wavelet modulus extreme values in the average value curve, manual errors or inaccuracy should be avoided. Thus, we employed the user-defined Eq. (1) which contained sum, absolute value, and mean value functions. Herein, n referred to the value at the n column. The modulus extreme value could be obtained via the formula, and according to nearby values, we could determine whether it was a maximum or minimum value.

$$y = (\mathrm{SUM}(\mathrm{ABS}(1:n)))/n \tag{1}$$

4. Results

4.1. Types and features of event sedimentation

According to fine-grained core observation and thin-section identification, diverse fine-grained event sedimentation was identified from the cored wells in the Dongying Sag, mainly including the slide-slump, turbidities, hyperpycnite, and tempestites. Different fine-grained event sedimentation showed obvious distinctions.

4.1.1. Slide-slump deposits

The slide-slump deposits were the sediments accumulated in a lower flat area under a series of trigger mechanisms, in which the

gravitational force on the sediment downward along the slope fails to overcome the internal cohesion of the deposit. Then, under the influence of self-gravity, the deposits already stored in the high slope were transported again and moved along in the manner of continuous or intermittent blocks (rigid solids) toward the bottom of the slope. Slide-slump deposits were common in the study area as deformation structures caused by them could be observed in cored wells such as Fanye 1, Niuye 1, Guan 17-Xie 10, and Niuxie 55 well. Convolute bedding and severe lamina deformation were major deformation structures. For example, (1) Convolute bedding: cores and thin sections observations showed that convolute bedding was continuously distributed in one layer, often forming closely arranged inclined folds or recumbent folds (Fig. 2a, b, c, d) with a thickness of 0.25–9 cm. Some laminas had severe deformation, whose mechanical property was plastic deformation (Yang et al., 2015; Yuan et al., 2016). (2) Severe laminae deformation: Core observation showed that overlying and underlying strata had abrupt contact (Fig. 2e, f, g), layer thickness between 5–10 cm, and the sliding surface could be seen at the bottom. The internal laminae had poor continuity compared with convolute bedding. Severe crumpled deformation was observed between laminae, part of which fractured into pieces of different sizes in deformed sediments (Fig. 2h), which marked the distinction from convolute bedding with continuous laminae.

Notably, the slide-slump deposits were not necessarily caused by earthquakes (Feng et al., 2017). It was proved that many were formed due to non-tectonic activities (Zhong et al., 2019).

Slide-slump deposits formed by tectonic activities have bad continuity of internal laminae and were often accompanied by soft sediments deformation like ground fractures, microfolding, syn-sedimen, flame structures, pillow structures, spheroidal structures, and liquefied breccia (Du and Yu, 2017). In contrast, those triggered by non-tectonic activities were small in size with good continuity and often folded into multi-layers vertically. The reason is that a large amount of deposited clay liquefied under weak waves or flows, and the sliding-sliding occurs due to the loss of the original fixed supporting force, forming deformation laminae with relatively good continuity, among which some laminae were highly symmetrical. According to previous research, deformation laminae with great symmetry were observed when sediments liquefied and were prone to plastic flows (Zhong et al., 2019). According to careful core observation and microscopic thin-section identification, abrupt contact was found in the deformation structures and between overlying and underlying strata formed by the slide-slump

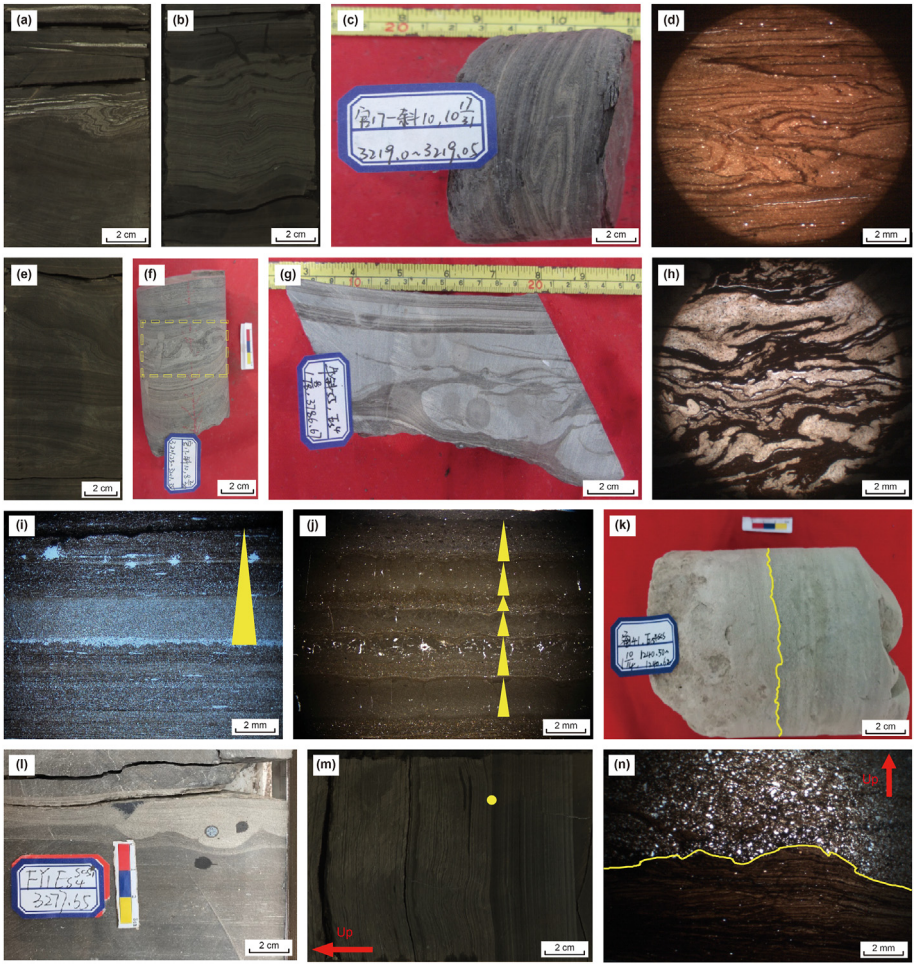

Fig. 2. Features of slide-slump deposit and turbidities. **(a)** Niuye 1 well with convolute bedding, 3374.81 m; **(b)** Fanye 1 well with convolute bedding, 3419.64 m; **(c)** Guan 17-Xie10 well with convolute bedding, 3219.03 m; **(d)** Niuye 1 well with convolute bedding, 3417.5 m, 1x(−); **(e)** Fanye 1 well with convolute bedding, 3339.70 m; **(f)** Guan 17-Xie10 well with laminae deformation, 3201.30 m; **(g)** Niuxie 55 well with slide-slump, 3786.67 m; **(h)** Niuye 1 well with laminae deformation, 3437.31 m, 1x(−); **(i)** Liye 1 well with normal graded bedding, 3604.41 m; **(j)** Niuye 1 well with multi-phase normal graded bedding, 3438.58 m; **(k)** Tong 41 well with scouring structure, 1240.60 m; **(l)** Fanye 1 well with load cast, 3277.65 m; **(m)** Scour surface was observed on the core of Fanye 1 well (at the yellow point), 3390.04 m; **(n)** Fanye 1 well. Abrupt change of clay rock to siltstone at the scour surface of the yellow dot in the picture (**m**), 3390.04 m, 5x (+).

in the study area. Besides, no other soft sediment deformation caused by earthquakes were discovered in the surrounding. The majority of deformation structures had good continuity with harmonious deformation internally and closed folds in some laminae. Recumbent folds occurred against strong slides; These folds were small in size at the height of 3–10 cm. Based on the characteristics above, it can be concluded that the slide-slump deposits resulted from the general movement due to the lack of support in the liquefied and destabilized sediments that had been accumulated on the slopes in the study area instead of under the influence of earthquakes.

4.1.2. Turbidities

Turbidity flow, a type of gravity flow, was formed at the bottom of a water body in high-speed turbulence, consisting of water and a large amount of self-suspended material (H. Jiang, 2010; Xu, 2014). According to recent studies, turbidity flows were the most important way to transport terrestrial clastic materials and other particles (Xu, 2013), carrying tremendous mud and sand into the deep ocean or lakes to form turbidites.

Our study area found turbidities in cored wells, including Fanye 1, Liye 1, Niuye 1, Tong 41, etc. The sedimentary characteristics were normal graded bedding, scouring structure, and load cast. (1) Graded bedding: The sediments at the bottom were coarse-grained and mostly siltstone in terms of normal graded bedding. Meanwhile, the grain size of sediments was finer upward, transiting to strips of silt clay (Fig. 2i). In addition, we observed sediments piled by multiple normal graded bedding due to multi-phase turbidity flows (Fig. 2j). (2) Scouring surface: The scouring structure was often accompanied by normal graded bedding. With an undulating morphology, its upper part often has coarse-grained siltstone and fine-grained clay rock can be noticed in the lower part, while abrupt contact came into being at the scour surface (Fig. 2k). (3) Load cast: Load cast appeared at the bottom of overlying sediments due to the rapid deposition, which generated considerable pressure on the underlying unconsolidated sediments (Fig. 2l).

4.1.3. Hyperpycnites

The hyperpycnal flow is a novel sedimentary transportation mechanism proposed in recent years (Tan et al., 2015), referring to a high-density fluid that flows along the bottom of the basin. As the hyperpycnal flow carried sediment particles, their fluid density was higher than that of stable ambient water and less influenced by buoyancy (Mulder and Syvitski, 1995). Overall, controlled by the flood dynamics, the hyperpycnal flows had similar dynamics characteristics and corresponding sedimentation features. Like flood hydrodynamics, hyperpycnal flows were first enhanced and then weakened (Mulder et al., 2003; Petter and Steel, 2006; Yang et al., 2015). The combination of inverse-normal graded bedding in hyperpycnites reflected that flood energy first weakened and then strengthened before finally declining. Besides, the hyperpycnite could develop climbing-ripple cross-lamination, parallel lamination, inner micro-erosion surface (Fig. 2b), plant fragments ("phytodebris") (Fig. 3c), and other sedimentary structures (Yang et al., 2015; Jin et al., 2019).

The hyperpycnites were found in the Chunshang Sub-member of Upper Es_4 in the cored wells of the study area, including Fanye 1 well, Tong 29 well, Wang 7 well, Wang 31 well, Wang 129 well, etc. The main sedimentary features included (1) Inverse-normal graded bedding structure: The inverse-normal graded bedding was composed of calcite particles or quartz particles in pairs with a thickness of 0.5–2.5 mm. Besides, the sediment particle size reached the maximum at the conversion surface, where no obvious erosion or deposition interruption was found (Fig. 3d), indicating the continuous change of flood hydrodynamics was the leading factor (Yang et al., 2015). (2) Climbing-ripple cross-lamination: the ripples climbed upward along the waterfront in the downstream direction, forming a lamination characterized by climbing or ascending trends (Fig. 3e), which reflected the sedimentation conditions of rapid periodical accumulation and the relatively slow flow velocity. (3) Corrugated beddings: According to the core and microscopic observation, such beddings are featured with either continuous or intermittent wave morphology and uneven thickness in different positions of the same laminae. Inside, mainly composed of calcite particles, quartz particles or clay with a thickness of 0.5–3 cm (Fig. 3b), corrugated beddings were formed mostly when the deposit rate was larger than the transport rate. (4) Carbonaceous debris: Hyperpycnite deposits were terrestrial sediments accumulated at the basin bottom by the flood. Therefore, plenty of terrestrial carbonaceous debris was among these deposits, which is a typical feature compared with other sedimentation. In the lime siltstone of Wang 31 well and Gongxie 27 well, it was found that carbonaceous debris was in layered or randomly uniform distribution, which marked the cause of hyperpycnite deposits. Layered distribution proved the sequence of deposits, carbonaceous debris after sandy debris, while the randomly uniform distribution showed that the deposition of two debris took place at the same time. (5) Low-angle cross bedding: Low-angle cross beddings were generated under weak hydrodynamics, often formed at the beginning stage of the flood enhancing period and the end of the weakening period. Such sediments were observed in the core wells of Wang 7 well and Fanye 1 well. The cores had lime or clay laminae, forming a skew of 2°–10° with the formation boundary (Fig. 3d).

4.1.4. Tempestites

Tempestites, a special type of sediments, usually develop between the normal-wave base and storm-wave base. The storm current changes primary water temperature and hydrodynamics while impacting allogenic and sedentary sediments. Meanwhile, the coarse-grained debris can be transported from shallow to deep water, forming high-energy sentiment under low-energy conditions (Zhong et al., 2020).

Storm currents could form various sedimentary structures, including erosional structures such as gutter casts and truncated structures, hummocky cross-bedding, wave-generated cross-bedding, graded bedding, massive bedding, wave ripples, and benthic escape. Tempestites were well developed in the study area, where tempestite characteristics and sequence, including truncation, wave-generated cross bedding, benthic escape, and coarse-grained stagnant bedding, were identified in Niuye 1, Wang 29, Fanye 1, and other wells.

(1) **Truncated structure** The truncated structure is a typical storm current indicator often in deep lakes with an irregular cutting surface, caused by the erosion and shearing of powerful storm current-back on sediments of the early period (Zhang et al., 2019). The truncated structure dip of Niuye 1 well was about 15°, which was relatively flat, and the overlying clay rock covered the microwave-shaped cutting surface.

(2) **Wave-generated cross bedding** The upper wave-generated cross beddings of Wang 129 well are composed of the herringbone structure of counterturn laminae or arranged in the convergence-confinement shape. In contrast, the lower beddings were featured with irregular waves (Fig. 4b). Wave-generated cross bedding proved that tempestites were developed on the normal-wave base (Zheng et al., 2010).

(3) **Benthic escape** Benthic escape in the wave-generated cross bedding was identified in Wang 129 well. The 5 mm-

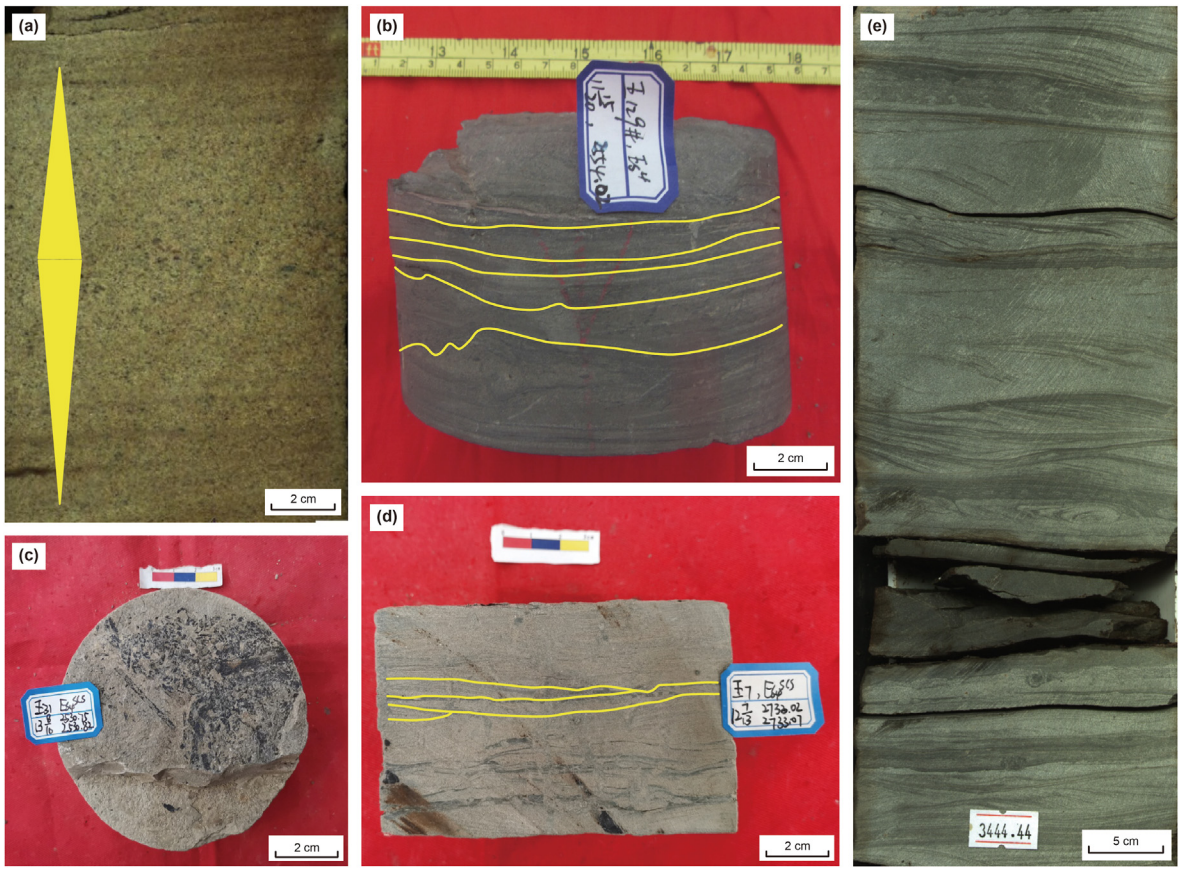

Fig. 3. Features of hyperpycnite deposits. **(a)** Inverse-normal graded bedding (Jin et al., 2019); **(b)** Wang 129 well, corrugated bedding, 2554.02 m; **(c)** Wang 31 well, carbonaceous debris, 2530.8 m; **(d)** Wang 7 well, low-angle cross bedding, 2733.5 m; **(e)** Climbing-ripple cross-lamination of Fanye 1 well, 3444.24–3444.44 m.

diameter wormhole was vertical to the bedding upward (Fig. 4c), indicating that the creatures had to escape upward when tempestites occurred to prevent burial. During the process, benthic escape was an important indicator of rapid deposit.

(4) **Coarse-grained stagnant bedding** Storm currents scoured and eroded the bottom sediments, which rapidly deposited under gravity due to their large density and coarse grains. Thus, the coarse-grained stagnant bedding became a representative characteristic of tempestites (Zheng et al., 2016). Coarse-grain stagnant bedding with a thickness of about 1 m can be seen in the core and thin section of Well Fanye 1, the lithology of coarse-grained stagnant deposits was calcarenite and bioclastic limestone. We observed a large amount of 0.4–1.2 mm arenite and bioclastic with poor roundness and sorting. Micritic limestone masses were observed partially after erosion, mainly supported by the micritic matrix (Fig. 4d).

(5) **Tempestites sequence** A relatively complete tempestite sequence was developed at 2555.2–2555.6 m in Wang 129 well, with the normally graded beddings, wave-generated cross-bedding, lens bodies, corrugated beddings and horizontal beddings from bottom to top, respectively (Fig. 4e). The hydrodynamic tended to decline after the storm peak period, and due to gravitational differentiation, the sediment became finer in size from the bottom up, forming normal graded beddings via regular sedimentation. Due to the flow and shape of the lake bottom affected by the storm, as the storm weakened, weak oscillatory flows and multi-directional flows often resulted in wave-generated cross bedding, a typical characteristic of tempestites and a sedimentary structure that vividly reflected the power of storms. Next, the water body energy continued to decrease, thus forming corrugated beddings. As deposition speed was faster than during storm breaks, the environment was unfavorable for biological activities, leading to rare trace fossils and biological disturbance inside. When the storm subsided, the water body calmed with low energy and fine-grained suspended materials gradually sedimented, forming the horizontal bedding.

4.2. Division of different-level astronomical cycles

In recent years, many scholars have worked to use various data and methods to extract the Milankovitch cycle in the Paleoproterozoic strata of the Dongying Sag: Tan et al. (2015) delineated 276 high-frequency cycles based on the superimposed features of logging curves, lithology and colour rhythms, and confirmed the existence of Milankovitch cycle signals by spectral analysis. Shi et al. (2019a, 2019b, 2020) first used magnetization rate as an alternative index to construct a high-resolution cyclostratigraphic framework for the lower third to the upper fourth section of the Shahejie Formation in the Bohai Bay Basin. Then they introduced EHA and ASM analyses techniques based on ordinary MTM spectral analysis, which determined the sedimentation rate to be 7.5–11.0 cm/kyr in the lower E_{S3} and the lower Ess_4 of the Dongying Sag, proving the existence of Milankovitch cycles in the Dongying Sag and identifying the long eccentricity, short eccentricity, obliquity cycles, and

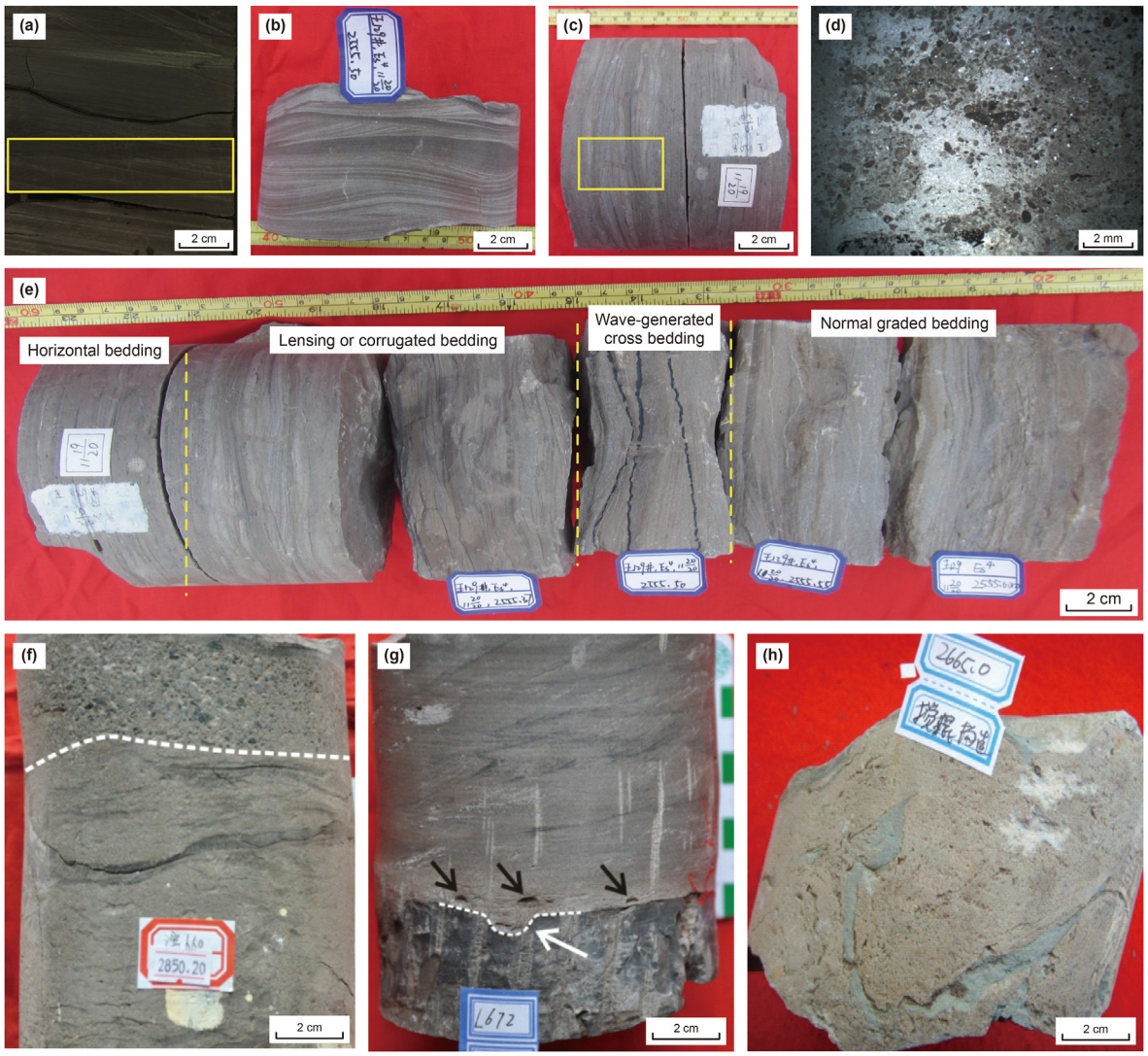

Fig. 4. Characteristics of tempestite. **(a)** Niuye 1 well with truncated structure, 3421.25 m; **(b)** Wang 129 well with wave-generated cross bedding, 2555.5 m; **(c)** Wang 129 well with benthic escape, 2555.4 m; **(d)** Fanye 1 well with coarse-grained stagnant deposit, 3436.94 m, 1x(−); **(e)** Wang 129 well with tempestite sequence. There was normal graded bedding, wave-generated cross bedding, lensing or corrugated bedding, and horizontal bedding from right to left, 2555.2–2555.6 m; **(f)** Bin 660 well with scouring surface structure and upper stagnant deposit, 2850.2 m (Wang et al., 2015a); **(g)** Li 672 well with scouring surface structure (white arrow) and claystone debris (black arrow), 4132.5 m (Wang et al., 2015a); **(h)** Bin 420 well with melange structure, 2665 m (Wang et al., 2015b).

precession cycles. Yu et al. (2021), Peng et al. (2022), Luan et al. (2022) and Zhou et al. (2022) also successively used correlation coefficient analysis, spectrum analysis, wavelet transform, power spectrum estimation and filtering analysis to conduct detailed studies on the paleozoic stratigraphy of the Dongying Depression. The results show that Chunshang Sub-member of Lower Es_3-Upper Es_4 has well-preserved Milankovitch cycles.

This work conducted the denoising and detrending pretreatment of the natural gamma log data in the study area, and the processed log data were subjected to spectral analysis. According to the results, the main cycle thicknesses were 31.672 m, 9.315 m, 4.061 m, 3.167 m, 1.65 m, and 1.466 m (Fig. 5), with the ratio of 21.6 : 6.353 : 2.769 : 2.16. 1.125 : 1 respectively, close to the ratio of orbital cycle 405 kyr : 124.22 kyr : 51.68 kyr : 39.76 kyr : 22 kyr : 18.82 kyr. Therefore, it could be concluded that the study area was controlled by eccentricity, slope, and precession cycle. In other words, the cyclic stratigraphy with the thickness of 31.672 m and 9.315 m corresponded to a 405 kyr long eccentricity cycle and a short 124.22 kyr eccentricity cycle, and the cyclonic strata with a thickness of 4.061 m and 3.167 m corresponded to 51.68 kyr and 39.76 kyr slope cycle, while the cyclic stratigraphy with the thickness of 1.65 m and 1.466 m corresponded to 22 kyr and 18.82 kyr precession cycle, respectively. This further confirms that the average sedimentation rate is 7.8 cm/kyr in the study section, which is consistent with the value of 7.5–11.0 cm/kyr obtained by Shi et al. (2019), thus proving the reliability of the Milankovitch cycles identified in this study. The power spectra were then analyzed to obtain the scale of the three local extreme points (Fig. 5), among which the ratio of scale values 163 and 51 equaled 3.20, similar to the ratio of long and short eccentricity cycle, 3.26. Therefore, the wavelet curves corresponding to the two-scale values could be viewed as the cyclic curves of the long and short eccentricity cycle. Based on the power spectrum estimation, we extracted the wavelet coefficient curves where the scale values were 163 and 51, respectively, to represent the cyclic curves of the studied interval. Finally, the study section identified 6 long and 22 short eccentricity cycles, 65.5 obliquity cycles, and 110.5 precession cycles via spectral analysis and power spectrum estimation methods (Fig. 6).

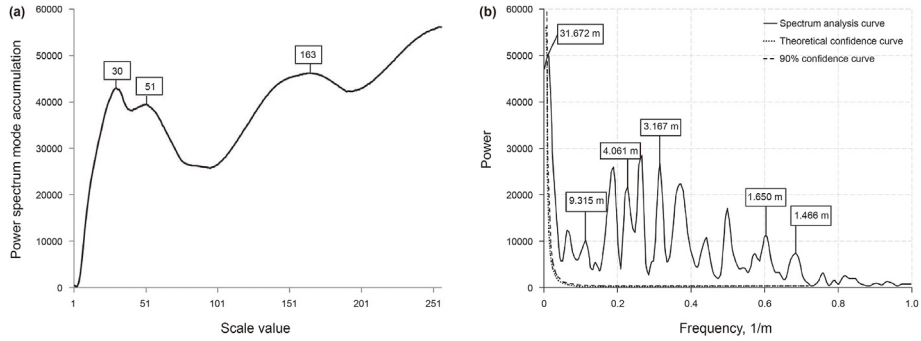

Fig. 5. **(a)** GR curve spectral analysis; **(b)** Wavelet analysis modulus extreme values of Chunshang Sub-member of Upper Es_4 in the Fanye 1 well.

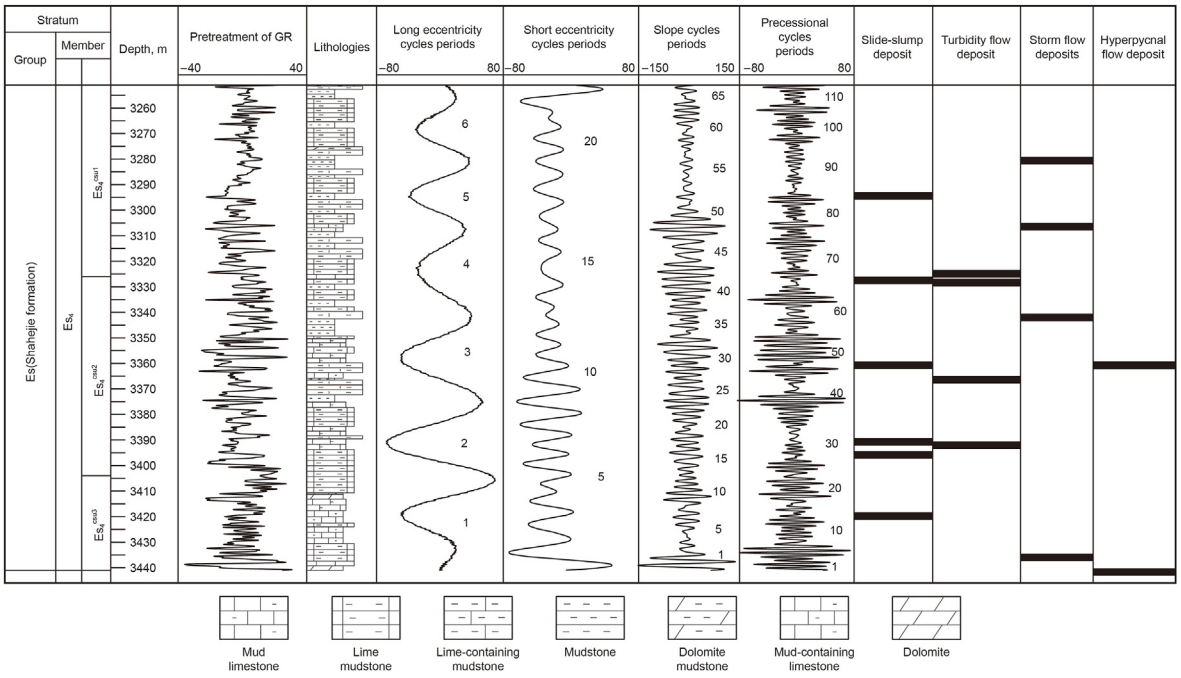

Fig. 6. The astronomical cycles period curve of Fanye 1 well in Chunshang Sub-member of Upper Es_4.

5. Discussion

5.1. Correspondence between astronomical cycles and event sedimentation

Based on event sedimentation characteristics and the division of different-level astronomical cycles in Chunshang Sub-member of Upper Es_4, the corresponding relationship between astronomical cycles and event sedimentation was further studied. As a result, when the maximum of the long eccentricity period transited to its minimum, the turbidities and slide-slump deposits were well developed, and when the minimum gradually changed to the maximum, the tempestites were well developed. The relationship between slope and precession cycle remains unclear in terms of the short eccentricity cycle (Fig. 6). Therefore, this study primarily discussed the control of the long eccentricity cycle on event sedimentation.

5.2. Control of long eccentricity period on event sedimentation

5.2.1. Climate

The long eccentricity cycle is critical to climate because it influences the amount and uniformity of solar radiation. When the eccentricity reached the minimum, the earth moving track around the sun was almost circular. The distance of perihelion was far from the sun, so the earth received little solar radiation, leading to a dry and cold climate. No obvious changes could be found among seasons, and the globe was in the ice age. When the long eccentricity reached the maximum, the orbit became elliptical, and the earth received plenty of solar radiation overall. Thus, the climate was warm and humid with obvious seasonal changes. The globe was in the interglacial stage (Wu et al., 2011).

Climate plays a crucial part in the formation mechanism of slide-slump and turbidity flows in lacustrine basins (Pietras et al., 2003; Renaut and Gierlowski-Kordesch, 2010; Zhang et al., 2016). Under dry climatic conditions, the sparse terrestrial vegetation and the strong erosion of surface sediments by rivers and rainfall (Allen et al., 1999) would lead to a high content of debris in rivers, tremendous of which will enter the lake and deposit on the slopes at the edge of the lacustrine basin, thus creating conditions for slide-slump and turbidity flows (Mulder et al., 1997). According to previous research (Leynaud et al., 2009; Pierau et al., 2010; Henrich et al., 2010; Urlaub et al., 2013), the arid climate could enhance slide-slump and turbidities in areas such as northwestern Africa and the European continental margin. In contrast, under warm and

humid climatic conditions, lush terrestrial vegetation consolidated soil and other sediments. Therefore, less debris in the rivers would give rise to fewer deposits in lakes, unfavorable to the generation of slide-slump and turbidities.

In addition to slide-slump and turbidities, climate largely affects storm currents. Generally, during the critical climate shifting period, global warming increases water temperature, a significant factor in forming storm currents (Huang and Liu, 2016). Additionally, global warming, sea-level rise, and monsoon offer favorable conditions for storm currents (Duke,1985; Emanuel,1987; Musgrave et al., 2008; Quan et al., 2012, 2014; Wang et al.,2013, Wang et al., 2015b). The prevailing monsoon during the geological history was essential to tempestites, and the tempestites of the Triassic and Jurassic in the western and northern Sichuan Basin were considered to have resulted from the strong monsoon at that time (Zhao et al., 2019; Zhong et al., 2021). The upper Es_4 of the Jiyang Depression was in a monsoon zone, often influenced by strong monsoon from the polar (Zhang et al., 2016; Jiang, 2018). Besides, during the upper Es_4 period, tempestites were observed in the Huimin Depression of Jiyang Depression (Zhang and Zhang, 2009) and the Dongying Sag (Wei et al., 2014; Wang et al., 2015a) (Fig. 4f, g, h).

Good correspondence was found between climatic conditions and carbonate mineral content as the solubility of calcium carbonate was negatively correlated to temperature. Under hot and dry conditions, evaporation was intense, and the evaporated water outnumbers the input. Thus, as calcium carbonate in water became supersaturated, calcite would be precipitated and deposited. When the climate was warm and humid, the evaporated water was less than the input, and calcium carbonate was unsaturated, impeding calcite precipitation. Therefore, the content of carbonate minerals in the deposit could reflect the paleoclimatic conditions during deposition. Moreover, paleoclimate could largely influence the dispersion and aggregation of elements. For example, considering that Na elements tended to migrate while Al elements were less likely to be affected during weathering (Jiang, 2010), the Na/Al ratio was often used to reflect the paleoclimate (Jin, 2017).

In this study, the Na/Al ratio and carbonate mineral content in long eccentricity cycles 1 and 2 as well as data from GR curves were adopted to analyze the relationship between event sedimentation and climate in the Chunshang Sub-member of Upper Es_4, combined with macroscopic core observations, thin section identification, and long eccentricity data (Fig. 7).

The minimum depth of long eccentricity cycle 1 was 3419 m. In terms of the geochemical index, the Na/Al reached the maximum at 3419 m, higher than the average 0.15 of this cycle, which reflects the arid and hot climate. Regarding mineral contents, the maximum carbonate mineral content was 70.1%, which was higher than the average 58.9% of this cycle, suggesting an arid and hot climate and intensified evaporation, where calcium carbonate in water was oversaturated, leading to carbonate precipitation and deposition. As for lithologies, argillaceous limestone and lime clay rock were developed at this depth. Based on core observation, the dark clay laminae and light-grey lime laminae were interbedded, while the latter ratio was higher than the former, which verified the climatic condition. Convolute bedding resulting from slide-slump was noticed at this depth, whose internal laminae were bent but with good continuity as it had abrupt contact with upper and lower dark-grey clay rock. The lack of proof for earthquake impacts suggested that destabilized sediments had slides and slumps due to liquefication. Both continuous and intermittent corrugated beddings caused by hyperpycnite deposits with a thickness of 0.2–2 cm were seen in cores at 3419.01 m and 3423.63 m, and their main contents were limes and clays. In addition, the climbing-ripple cross-lamination with a thickness of 0.5–1.5 cm was recognized at 3444.24–3444.44 m. The latter climbed over the former beddings, which reflected that at the beginning or end of storms, the sedimentary rate was larger than the transport rate.

The minimum depth of long eccentricity cycle 2 was 3390.8 m. In terms of geochemical index, the Na/Al reached the maximum 0.16 at 3389.5 m, higher than the average 0.12 of this cycle. The maximum carbonate mineral content was 51.5% in mineral contents, higher than the average 49% of this cycle. Regarding lithologies, thick mud-containing limestone was observed, which contained thin sections of lime-containing clay rock, indicating the arid and hot climate during deposition. Besides, near this depth, we found two sections of the combined convolute bedding and massive structure in abrupt contact caused by slide-slump. The convolute bedding was 4 cm in height and composed of thick light-grey lime laminae and thin dark-grey clay laminae with continuous deformation in internal laminae, proving that destabilized sediments had slides and slumps due to liquefication. One scouring surface affected by turbidities was also observed at a similar depth (Fig. 2m, n). Notably, the internal laminae of the convolute bedding at 3389.53–3389.73 m was inclined at an angle of 15°, presumably due to the slide-slump effect of unconsolidated sediments on the slope. The lithology of the blocky structure was dark-grey clay rock with homogeneous blocky mass, undeveloped laminae, and high organic matter content, which could be caused by deposition following the slide-slump effect. The scour surface structure formed by turbidity flows could be seen at 3390.04 m in Fanye 1 well (Fig. 2m). The microscopic observation showed that the scour surface was irregular with laminae clay rock in the lower part and massive siltstone in the upper part, equivalent to section A of the Baoma sequence. Abrupt contact was observed between siltstone and clay rock, and debris of the latter was inside the blocky siltstone (Fig. 2n). Thus, it could be inferred that the turbidity flow with strong energy eroded the lower sediments and involved sediment debris.

In addition, multi-period tempestites were observed near the maximum of the long eccentricity cycle (Fig. 8). The depth at the maximum of long eccentricity cycle 1 was 3432 m, with argillaceous limestone and lime clay rock as major lithology. The corresponding Na/Al value was 0.13, which was lower than the average 0.15 of this cycle, and the carbonate mineral content was 45.59%, which was much lower than the average value of 58.9% in this cycle. The maximum depth of eccentricity long period 2 was 3405.28 m, and the lithology was mainly lime clay rock with a minimum carbonate minerals value of 17.03%, which was much lower than the average 49% in this cycle, indicating higher humidity at the maximum than other periods in the cycle.

Four sections of tempestites were developed at 3429.84–3430.84 m (Fig. 8a):

(1) 3430.56–3430.84 m: 14 cm massive limestone was developed in the lower part, and 8 cm coarse-grained stagnant bedding at the bottom. A large quantity of debris was arranged disorderly inside, and the number of debris and size of sediments reduced with the decrease of depth, forming normal graded bedding. The upper part was transformed into 14 cm corrugated laminae limestone with continuous and intermittent beddings.
(2) 3430.5–3430.56 m: 6 cm massive structure was developed. At the bottom formed an uneven erosion surface due to the storm, where limestone was above, and the broken clay debris was in a random distribution inside. As the storm intensity weakened upward, the clay content increased and argillaceous limestone came into being.
(3) 3430.39–3430.5 m: The lithology was argillaceous limestone. The bioturbation structure formed by the rapid

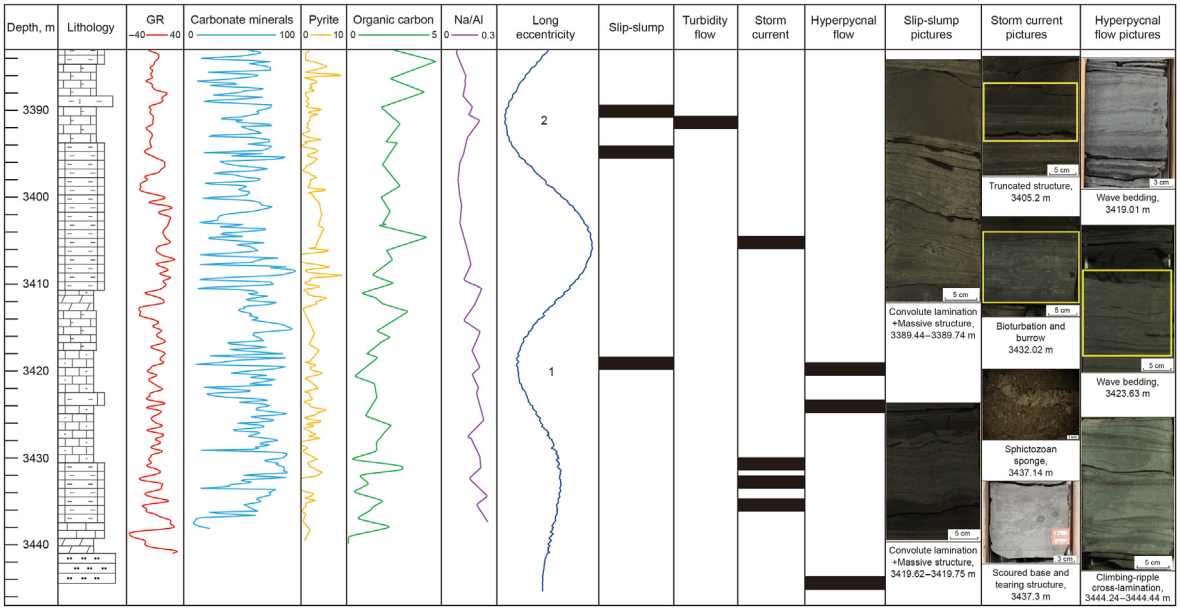

Fig. 7. Relationship between event sedimentation and climate in long eccentricity cycles 1 and 2 in the Chunshang Sub-member of Upper Es_4 in the Fanye 1 well.

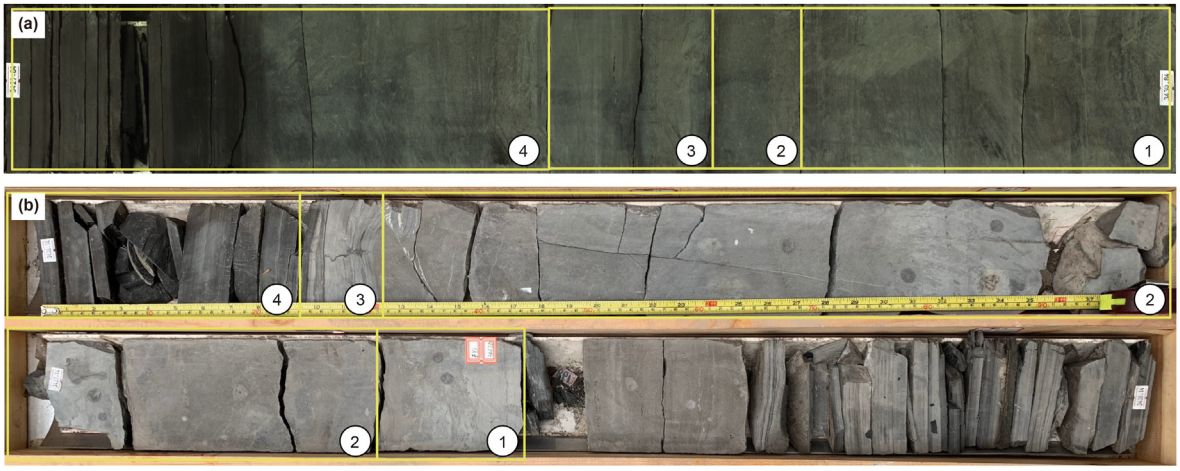

Fig. 8. Deposit sequence of storm currents in Chunshang Sub-member of Upper Es_4 in the Fanye 1 well **(a)** Tempestites in Fanye 1 well at 3429.84–3430.84 m; **(b)** Tempestites in Fanye 1 well at 3436.14–3437.61 m.

sedimentary event was at the bottom 4 cm, and the bioturbation resulted in the uneven distribution of clayey materials, which were mostly clumps and blocks in the concentrated distribution of the argillaceous limestone, representing the products formed at the beginning of storms. In the middle 5 cm, continuous corrugated beddings were noticed with a thickness of about 0.8 cm. Upward, the hydrodynamic force gradually weakened, and the sedimentary structure of the top 2 cm turned into massive beddings from corrugated ones.

(4) 3429.84–3430.39 m: The laminae were destroyed and broken by the bioturbation structure and biological drilling at the bottom 5 cm. In the middle, the massive structure was formed through the effect of the storm, and the lenticular body was developed internally after the calcite laminae were broken by the storm. In the upper 20 cm, massive dark grey claystones were found, representing the products forming during the storm retreating period.

By observing the core and thin sections, we identified a relatively complete tempestite sequence in Fanye 1 well at 3436.14–3437.61 m (Fig. 8b):

(1) The 20 cm silty limestone was found at the bottom of the tempestite sequence, while the eroded bottom and tearing structures existed on the core, suggesting severe disturbance deformation. The erosion caused the uneven and undulating eroded bottom of the storm bedding, scouring, and etching of sand, ostracum, or bioclastic carried by strong storm whirlpool and flows on the surface of the preceding sediment during the storm strong stage (Liu et al., 1986). To a certain extent, the magnitude of the unevenness reflected the strength of the storm current.

(2) In the middle of the tempestites, coarse-grained stagnant bedding with a thickness of about 1 m was seen on the core and in the thin section, and its lithology was calcarenite and bioclastic limestone. Herein, many poorly sorted and rounded bioclastic and arenite were found with a size of 0.4–1.2 mm (Fig. 4d), revealing relatively rapid deposit speed. Besides, the matrix was micritic calcite. The coarse-grained stagnant bedding was next to the eroded bottom surface, a typical feature of tempestites (Lin et al., 2008). At the strong stage of the storm current, the storm whirlpool undercut, lifted, stirred, and deposited along the bottom after transporting a short distance. The sphinctozoa caused by storm transportation and deposition could be seen in calcarenite, reflecting the warm climatic conditions at that time (Deng, 2016).

(3) A limestone laminae about 6 cm thick was deposited on top of the coarse-grained stagnant bedding, where a hummocky cross bedding of 2–3 cm thickness was developed. Previous studies suggested that the tempestites with coarse clastic layers indicated a shallow depositional environment of water bodies and stronger storm currents. In addition, the tempestite sequence was generally incomplete, but the eroded structures and hummocky cross bedding were developed, whose lithology was mainly bioclastic limestone (Zhang et al., 2019).

(4) A 20-cm-thick clay rock with horizontal laminae was developed at the top of the tempestites, which were products unloaded from the clayey suspended components in the water body during the storm current interval (Ma et al., 2017).

The truncated structure (Fig. 7) was identified in the core at 3405.2 m near the maximum depth of long eccentricity period 2, with an irregular and corrugated truncated surface. The grey and straight-laminae clay-containing limestone was beneath the truncated surface, and the dark grey massive claystone was above. Thus, it indicated that the straight laminae of the underlying clay-containing limestone were sheared and eroded by the backflow of the storm. When the storm ended, the claystone covered the truncated surface in normal weather conditions.

In addition, the massive structures formed by storms were identified at 3343.25 m and 3373 m near the maximum depth of long eccentricity periods 3 and 4 (Fig. 9). Plenty of calcite and biological debris was found in the massive structure at 3343.25 m with mixed sizes ranging from 1 to 165 μm and poor sorting and roundness, which reflected that the storm current lifted, tore, and broke the off-site unconsolidated sediments, some of which were carried away. When the storm subsided, these fragments accumulated rapidly at the bottom. The massive structure at 3373 m differed in that a large number of calcite lenticular bodies were developed internally, and a small amount of silt was distributed uniformly. Meanwhile, the long axis of lenticular bodies lined up horizontally, with their size significantly decreasing twice from bottom to top, which indicated that the storm broke the calcite bedding that had been deposited first and then formed lenticular bodies, which were further deposited and compacted due to gravity.

Analysis showed that small long eccentricity could impede the growth of terrestrial vegetation, and the rivers and rainfall tend to erode terrestrial surface sediments, which might deposit at the edge of the lacustrine basin or further away along with the flow. Under certain triggering mechanisms, slide-slump deposits or turbidities came into the study area. Meanwhile, water and soil loss, accompanied by periodical flood, was likely to happen in provenance areas under arid climatic conditions, thus greatly enhancing the suspended materials in rivers and improving the likelihood of hyperpycnal flows. In addition, the long eccentricity period also hugely affects the tempestite. When the long eccentricity was large, the movement trajectory of the earth around the sun became flat, and the earth was closer to the sun at perihelion. During the hot summer, the thermal contrast was high between the surface, lakes, and land, and the monsoon tended to be powerful (Kutzbach et al., 2008; Wang and Ding, 2008;). Modern climate studies have shown that monsoon is closely related to storm currents. During the monsoon onset and offset, the frequency of storm currents showed a significant increase due to the smaller vertical shear of wind speed (Islam and Peterson, 2009; Van Loon, 1990; Lv, 2017; Yan et al., 2020). According to stalagmite $\delta^{18}O$ isotope data, the monsoon intensity increased with solar radiation during the geological-historical period (Cheng et al., 2009), and the prevailing monsoon was the premise for tempestites formation (Zeng et al., 2011). Overall, in the Chunshang Sub-member of the Upper Es_4, the eccentricity value was large, and the earth received sufficient solar radiation, leading to a warm and humid climate that created conditions for the monsoon onset, which thus contributed to the occurrence of storm currents and typhoon. Finally, the tempestite was formed in the Chunshang Sub-member of Upper Es_4 in the Fanye 1 well.

5.2.2. Water depth

The astronomical cycle plays a significant role in controlling water depth (Allan and Matthews, 1982; Elrick and Scott, 2009; Wang et al., 2018; Shao et al., 2021; Li et al., 2021). Studies pointed out that the moderating effect of eccentricity is the main driving mechanism of sea (lake) level changes (Boulila et al., 2010; Huang, 2014; Mei, 2015). For instance, good correspondence between paleolake area changes and eccentricity changes could be observed during the Cenozoic Era of Ebro Basin in Portugal, the Pliocene of Cadiz Bay in Spain, the Miocene of Guide Basin in Qinghai and Tarim Basin in Xinjiang, the Jurassic of Junggar Basin in Xinjiang, and the Eocene of Bohai Bay Basin (Sierro et al., 2000; Valero et al., 2014).

Event sedimentation is bound up with the changes in water depth. Bouma (2004) suggested that sediments were more easily transported to the interior of basins in the form of gravity flow at low sea levels (Li et al., 2021). Researchers confirmed the significance of water depth in controlling the development of gravity flow after the detailed study of deep-water gravity flow in Yinggehai Basin, Songliao Basin, Bohai Bay Basin, Pearl River Mouth Basin, Lower Congo-Congo Fan Basin, and other regions (Pang, 2012; Huang et al., 2018; Feng et al., 2018; Zhao et al., 2019; Xing et al., 2020; Chen et al., 2021a,b).

The water depth changes could be reflected by the organic carbon content in the sediments. The increased organic carbon content in the sediments indicates a warm-humid, high-water-level climatic environment, while the decreased one reveals a dry-cold, low-water-level climatic environment with the sediments getting close to the water surface (Tyson, 2001; Ding et al., 2015). Particular authigenic minerals like pyrite could also reflect the paleowater depth to some extent. The pyrite content was proportional to the water depth. In other words, deeper water led to higher pyrite content (Yang et al., 2019; Wu et al., 2018).

The study utilized the contents of organic carbon and pyrite in long eccentricity periods 3 and 4 for analyzing the relationship between event sedimentation and water depth of Fanye 1 well in the Chuanshang sub-member of the upper Es_4 (Fig. 9) with the support of materials collected by macroscopic core observation and microscopic thin section identification, as well as the data of long eccentricity.

The average contents of organic carbon and pyrite were 2.4% and

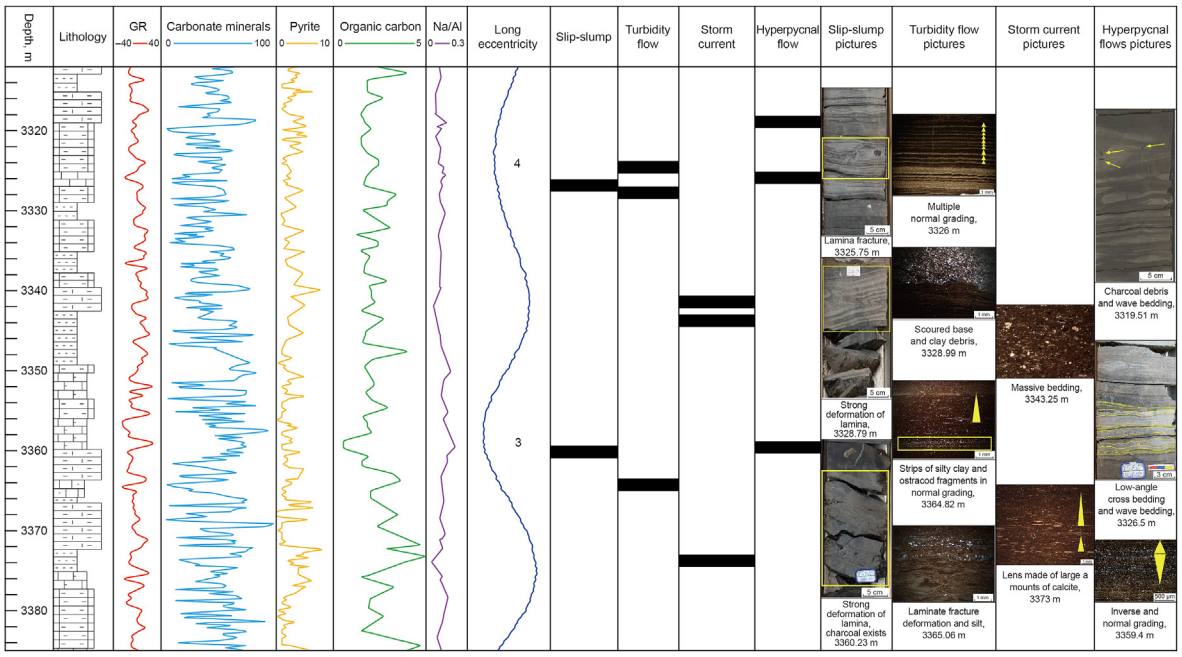

Fig. 9. The relationship between event sedimentation and water depth of Fanye 1 well in the Chunshang sub-member of upper Es_4.

2.45%, respectively, in a long eccentricity period of 3. At the maximum of long eccentricity, the contents of organic carbon and pyrite were 4.8% and 4%, and the lithology was mainly developed as clay rock and lime-containing clay rock; while near the minimum, the organic carbon content and the pyrite content were as low as 0.51% and 1.59%, and the lithology was turned into lime clay rock and clay-containing limestone. The relative contents of carbonate minerals and clay minerals can manifest the depth of water: the shallower the water, the more carbonate minerals, and the fewer clay minerals (Du et al., 2016; Peng et al., 2020). Through the core and thin section observation, the logging curve of the silt-containing clay rock at 3359.4 m near the minimum of the long eccentricity period 3 was finger-shaped, which was inferred to be caused by hyperpycnal flows (Zhou et al., 2020). The inverse-normal graded bedding structure was formed internally due to the hyperpycnal flow. The lower part has relatively low siltstone content, and the siltstone content gradually increased upward, forming an inverse-graded bedding. When the siltstone content reached the maximum, the clay increased, and the siltstone declined, forming normal graded bedding. The two beddings had gradational contacts. There was severe laminae deformation and convolute bedding due to slide-slump at 3325 m and 3360 m, whose characteristics were: abrupt contact between overlying and underlying beddings and a slope in the core. Besides, a small amount of charcoal debris was observed inside, reflecting its sliding along the shear surface. As the slide-slump proceeds, the water-saturated sediment was gradually liquefied, and the sediment rotated due to shearing, gradually intensifying the deformation of some laminae and ultimately resulting in fractures with the mechanical property of plastic deformation (Wang, 1991; Yang et al., 2015; Yuan et al., 2016). In addition, we observed that lime and clay laminae transformed into convolute bedding due to fold deformation in the thin layers, which reflected the process of contemporaneous deformation caused by gravity destabilization in the internal laminae (Fu et al., 2021). There was no soft-sediment deformation formed by earthquakes in the surrounding, revealing that liquefication and the loss of stability were the cause of slide-slump at this depth. Strips of silt clay were developed in the horizontal layer at 3364.82 m of core thin section bottom, corresponding to section D of the Baoma sequence. The clay content increased upward, gradually transiting into section E, where ostracoda pieces were arranged in a positive horizontal rhythm, revealing the decline of turbidity flow energy and speed and reflecting the features of graded sediments. In the argillaceous limestone at 3365.06 m of Fanye 1 well, severe deformation and fracture occurred in the laminae, leaving plenty of silt in the upper fractured laminae. Silt particles were mostly well-rounded and sorted, being round or sub-rounded. Turbidity flow events might be a major cause of such deposits, which was often related to decreasing water depth and increased hydrodynamics (; Wang et al., 2020).

The average contents of organic carbon and pyrite were 2.09% and 2.98% in the long eccentricity period 4. During the transition of long eccentricity from the maximum to the minimum, the contents of organic carbon and pyrite fell to 1.7% from 2.2%, and to 1.5 from 4.9%, respectively. The lithology was turned into lime clay rock and thin-layer limestone from clay rock and lime-containing clay rock, which demonstrated that the water got shallower when the long eccentricity moved from the maximum towards the minimum. The core and thin section observation found that near the minimum of long eccentricity, more severe deformation and fractures of laminae were induced by slide-slump at 3325 m in long eccentricity period 4 (Fig. 9). At a depth of 3328.79 m, a 5-cm-thick tightly closed recumbent fold was observed in the laminae. With a horizontal shortening coefficient of about 2, its length changed from 20 cm to 10 cm or so. The internal laminae, however, remained continuous and complete, proving its great plasticity during deformation and external conditions for continuous deformation.

Moreover, without earthquake action proof nearby, this tightly closed recumbent fold was speculated to be caused by the instability due to a large number of liquified sediments. Argillaceous limestone showed multi-phase normal graded bedding in the thin core section at 3326 m, reflecting frequent turbidity flows during this period. Siltstone thin layers caused by turbidity flows were identified in the thin sections at 3328.99 m, and abrupt contact was observed in the lower lime clay rock. Microstrip-shaped scour

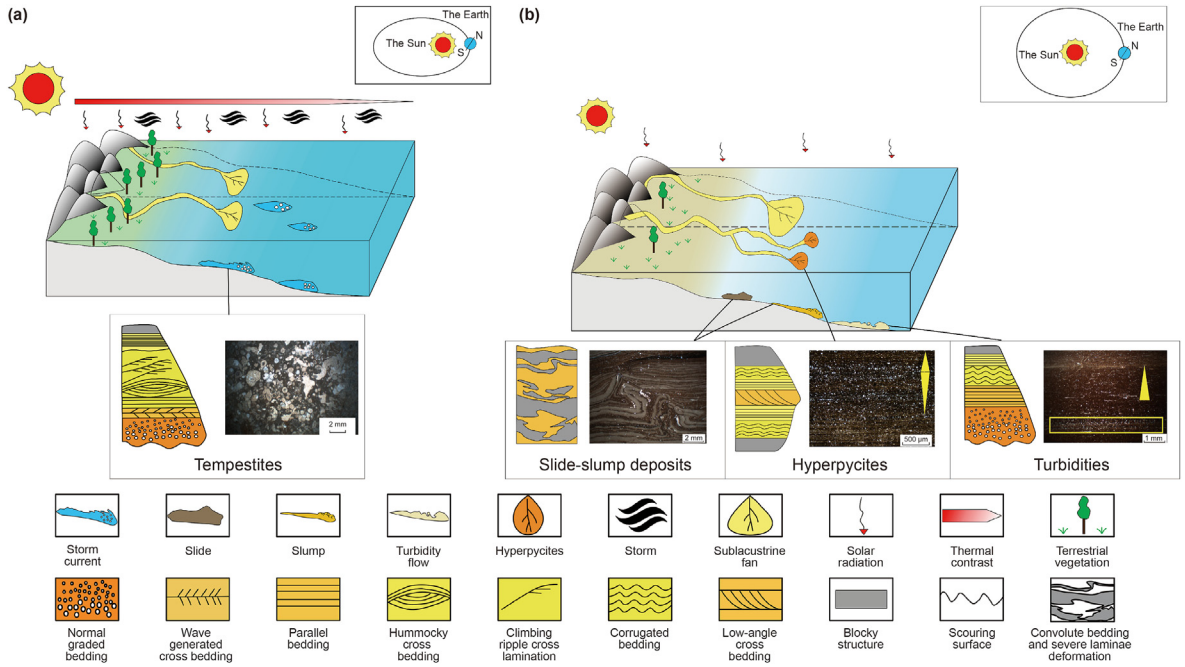

Fig. 10. Event sedimentation development model under the control of long eccentricity period. (**a**) The development model of event sedimentation controlled by large long eccentricity periods; (**b**) The development model of event sedimentation controlled by small long eccentricity periods.

surface was developed between them. Clay rock debris was surrounded by siltstone at the bottom, which suggested relatively strong turbidities eroded the clay rock basis and involved eroded pieces. Similar depositional features were discovered in the mud shales of the Nenjiang Formation of the Songliao Basin and the Wufeng Formation-Longmaxi Formation of the Sichuan Basin, all of which were considered typical turbidities. A 26 cm thick intermittent corrugated bedding was observed at 3319.51 m with a small amount of terrigenous carbonaceous debris scattering inside, which proved that hyperpycnal flows were the cause of corrugated bedding. The corrugated bedding and low-angle cross bedding caused by hyperpycnal flows were observed at about 3326.5 m, which featured interbedded corrugated lime laminae and clay laminae and abrupt contact. The relatively thick lime laminae ranging from 1 to 3 cm had a continuous and corrugated morphology, with a thin low-angle cross bedding of about 0.5 cm thickness and a 2°–5° angle in the upper part.

Analysis showed that when the long eccentricity was small for long eccentricity periods 3 and 4, the climate was dry and cold with low precipitation. Meanwhile, the lake evaporated more than its weak terrestrial input, gradually decreasing the lake level. With the decline, the denudation intensified, and the input of terrestrial detrital material transported by rivers increased. A large number of sediments were carried by the river towards lacustrine basins and accumulated on the slope zone of deltaic front in the steep northern slope of the Dongying Sag, and part of those sediments continued moving until they were deposited in a half-deep lake, providing the material basis for the emergence of gravity flow; meanwhile, during the rapid decline of lake level, the early sediments were more likely to induce gravity flow events under external forces owing to the swift lessening of pressure from overlying water body and the lower shear bond strength (Wang et al., 2015b). In addition, with the continuous sedimentation in the slope zone of the deltaic front, the thickness and critical angle of the sedimentary layer became larger, and sediments were more prone to be liquified under the effect of lake waves or currents, which increased the likelihood that the sediments collapsed under the influence of gravity to form the event sedimentation such as slide-slump and turbidities. Furthermore, with the lake level dropped, the height difference between rivers and catchment basins increased, then the accommodating space of basins contracted, and the sediments flowed along the existing canyon channels or the hyperpycnite channels arising from erosion. At the same time, the jacking force of the lake to the river was reduced and the deposit carried by the river was unloaded into the basin, facilitating the development of hyperpycnites in the deep lake.

6. The development model of event sedimentation controlled by long eccentricity periods

The study showed that the long eccentricity periods controlled event sedimentation, including tempestites, slide-slump, turbidities, and hyperpycnites.

When the long eccentricity was large, the earth at perihelion was closer to the sun, and more solar radiation arrived at the surface of the earth, creating a larger thermal difference and a warm-humid climate, which were closely related to the monsoon onset. Frequent monsoon activities provide good conditions for storm currents. Therefore, tempestites often happened when the long eccentricity was large (Fig. 10a).

When the long eccentricity was small, the earth at perihelion was far from the sun, and less solar radiation arrived at the surface, leading to a dry-cold climate featuring little rainfall followed by declined lake level, stunted and sparse terrestrial vegetation. Besides, the serious loss of water and soil in provenances led to a high concentration of suspended substances in rivers, favorable to forming hyperpycnites. In the meantime, a portion of sediments was deposited on the slope zone at the edge of lacustrine basins, offering the material basis for the generation of slide-slump and turbidities. With the further accumulation of sediments and continuous diminution of water depth, the thickness and critical angle of deposits increased while the internal shear bond strength decreased. Meanwhile, the sediments would liquify under

extremely weak lake waves or currents and lose the supporting force for fixation, bringing about the collapse of sediments under gravity and the event sedimentation, such as slide-slump and turbidities (Fig. 10b).

7. Conclusions

This study selected the Chunshang Sub-member of the Upper Es_4 in Dongying Sag Bohai Bay Basin as the research object and adopted core observation, thin section authentication, and XRD of whole rocks to identify the event sedimentation of fine-grained deposits in the lacustrine basin. Spectral analysis, power spectrum estimation, and extreme modulus values were used to analyze the astronomical cycle of the studied beddings, the lacustrine fine-grained event sedimentation, and response characteristics of the astronomical cycle orbit. The conclusions are as follows.

(1) With macroscopic core observation and microscopic thin section identification, we found turbidities, hyperpycnites, slide-slump deposits, and tempestites in the study area.
(2) According to the spectral analysis, power spectrum estimation, and extreme modulus values, we observed 6 long eccentricity periods, 22 short eccentricity periods, 65.5 obliquity cycles, and 110.5 precession cycles.
(3) When the long eccentricity was large, frequent monsoons created favorable conditions for the occurrence of storms, so the tempestite was developed during this period. When the long eccentricity was small, vegetation was stunted and sparse terrestrial, and surface sediments were severely eroded by rivers and rainfall, conducive to developing slide-slump deposits, turbidities, and hyperpycnites. Relationships between the event sedimentation and short eccentricity periods, obliquity cycles, and precession cycles remain unclear and need further research.

Declaration of competing interest

The authors declare that they have no known competing financial interests or personal relationships that could have appeared to influence the work reported in this paper.

Acknowledgements

This study was supported by the Study on Astronomical Stratigraphic Period of Lacustrine Shale and High Resolution Sedimentary Cycle in Logging (41872166) of the National Natural Science Foundation of China and the Exploration and Development Research Institute, Shengli Oilfield Company, SINOPEC.

References

Allan, J.R., Matthews, R.K., 1982. Isotope signatures associated with early meteoric diagenesis. Sedimentology 29, 797–817. https://doi.org/10.1111/j.1365-3091.1982.tb00085.x.

Allen, J., Brandt, U., Brauer, A., Hubberten, W., Huntley, B., Keller, J., Kraml, M., Mackensen, A., Jens, M., Negendank, J.F.W., Nowaczyk, N.R., Oberhänsli, H., Watts, W.A., Wulf, S., Zolitschka, B., 1999. Rapid environmental changes in southern Europe during the last glacial period. Nature 400, 740–743. https://doi.org/10.1038/23432.

Boulila, S., Galbrun, B., Hinnov, L.A., Collin, P.Y., Ogg, J.G., Fortwengler, D., Marchand, D., 2010. Milankovitch and sub-milankovitch forcing of the oxfordian (late jurassic) terres noires formation (se France) and global implications. Basin Res. 22, 717–732. https://doi.org/10.1111/j.1365-2117.2009.00429.x.

Bouma, A.H., 2004. Key controls on the characteristics of turbidite systems. Spec. Publ.-Geol. Soc. 222, 9–22. https://doi.org/10.1144/GSL.SP.2004.222.01.02.

Cao, Y.C., Jin, J.H., Liu, H.N., Yang, T., Liu, K.Y., Wang, Y.Z., Wang, J., Liang, C., 2021. Deep-water gravity flow deposits in a fault lake basin and their oil and gas geological significances in eastern China. Petrol. Explor. Dev. 48, 247–257. https://doi.org/10.1016/S1876-3804(21)60023-X.

Chen, H., Lin, C.S., Zhang, Z.M., Zhang, D.M., Li, M., Wu, G.K., Zhu, Y.X., Xu, H., Lu, W.M., Chen, J.H., 2021a. Evolution and controlling factors of the gravity flow deposits in the Miocene sequence stratigraphic framework, the Lower Congo Congo Fan Basin, West Africa. Petrol. Explor. Dev. 48, 127–138. https://doi.org/10.1016/S1876-3804(21)60011-3.

Chen, H., Lin, C.S., Zhang, Z.M., Zhang, D.M., Zhu, Y.X., Wu, G.K., Li, M., Xu, H., Guo, R.T., 2021b. Depositional characteristics and evolution of Miocene deep-water channel systems in block A of lower Congo-Congo Fan Basin, west africa. Pet. Geol. Exp. 43, 476–486. https://doi.org/10.11698/PED.2021.01.11 (in Chinese).

Cheng, H., Fleitmann, D., Edwards, R.L., Wang, X.F., Cruz, F.W., Auler, A.S., Mangini, A., Wang, Y.J., Kong, X.G., Burns, S.J., Matter, A., 2009. Timing and structure of the 8.2kyr B.P. event inferred from δ180 records of stalagmites from China, Oman, and Brazil. Geology 37, 1007–1010. https://doi.org/10.1130/G30126A.1.

Deng, Z.Q., 2016. Permian fossil sponges from rutog of Western Xizang, China. Acta Palaeontol. Sin. 433–438. https://doi.org/10.19800/j.cnki.aps.2016.04.003.

Der Meulen, B.V., Gingerich, P.D., Lourens, L.J., Meijer, N., Van, B.S., Van, G.S., Abels, H.A., 2020. Carbon isotope and mammal recovery from extreme greenhouse warming at the Paleocene–Eocene boundary in astronomically-calibrated fluvial strata, Bighorn Basin, Wyoming, USA. Earth Planet Sci. Lett. 534, 1–11. https://doi.org/10.1016/j.epsl.2019.116044.

Ding, X.J., Liu, G.D., Zha, M., Huang, Z.L., Gao, C.H., Lu, X.J., Sun, M.L., Chen, Z.L., Zhuang, L.X., 2015. Relationship between total organic carbon content and sedimentation rate in ancient lacustrine sedi-ments, a case study of erlian basin, northern China. J. Geochem. Explor. 149, 22–29. https://doi.org/10.1016/j.gexplo.2014.11.004.

Duke, W.L., 1985. Hummocky cross-stratifification, tropical hurricanes, and intense winter storms. Sedimentology 32, 167–194. https://doi.org/10.1111/j.1365-3091.1985.tb00502.x.

Du, X.B., Liu, H., Liu, H.M., Lu, Y.C., Wang, Y., Hao, X.F., Yang, W.Q., Ding, J.H., 2016. Methods of sequence stratigraphy in the fine GrainedSediments: a case from the upper fourth sub memberand the lower third sub member of the ShahejieFormation in well Fanye 1 of dongying sag. Geol. Sci. Technol. Inf. 35, 1–11. CNKI:SUN:DZKQ.0.2016-04-002(in Chinese).

Du, Y.S., Yu, W.C., 2017. Earthquake-caused and non-earthquake-caused soft-sediment deformations. J. Palaeogeogr. 19, 65–72. https://doi.org/10.7605/gdlxb.2017.01.005 (in Chinese).

Elrick, M., Scott, L.A., 2009. Carbon and oxygen isotope evidence for high-frequency (10 4 –10 5 yr) and My-scale glacio-eustasy in Middle Pennsylvanian cyclic carbonates (Gray Mesa Formation), central New Mexico. Palaeogeogr. Palaeoclimatol. Palaeoecol 285, 307–320. https://doi.org/10.1016/j.palaeo.2009.11.023.

Emanuel, K.A., 1987. The dependence of hurricane intensity on climate. Nature 326, 483–485. https://doi.org/10.1038/326483a0.

Fu, J.H., Li, S.X., Niu, X.B., Deng, X.Q., Zhou, X.P., 2020. Geological characteristics and exploration of shale oil in chang 7 member of triassic yanchang formation, ordos basin, NW China. Petrol. Explor. Dev. 47, 870–883. https://doi.org/10.11698/PED.2020.05.03 (in Chinese).

Fu, Y., Li, Z.C., Wan, P., Que, Y.J., Wang, Z.J., Ji, Y., Huang, L., Luo, J.L., Bao, Z.D., 2021. Sedimentary characteristics and controlling factors of slump gravity flow in delta front:a case study of Qing 1 member in Da'an area,Songliao Basin. Lithol. Reservoirs 33, 198–208. https://doi.org/10.12108/yxyqc.20210118 (in Chinese).

Feng, Y.L., Zou, C.N., Meng, Q.A., Wu, W.A., Lu, W.H., Zhu, J.Y., 2018. Tectonic and climatic influences on architecture of sequences and sedimentary systems in a post-rift basin: insight from late cretaceous northern Songliao Basin. Earth Sci. 43, 3445–3461. CNKI:SUN:DQKX.0.2018-10-010(in Chinese).

Feng, Z.Z., Bao, Z.D., Zheng, X.J., Wang, Y., 2017. Researches of soft-sediment deformation structures and seismites in China: a brief review. J. Palaeogeogr. 19, 7–12, 0.7605/gdlxb.2017.01.002(in Chinese).

Gao, Y., Fu, X.G., Wan, Y.L., Wang, Z.W., Song, C.Y., Li, X.R., 2020. Development features and controlling factors of mixed siliciclastic-carbonatesediments in the member 3 of the quemocuo formation, northern QiangtangBasin. J. Northwest. Polytech. Univ. 44, 45+106+7. https://doi.org/10.3969/j.issn.2095-4107.2020.03.004 (in Chinese).

Henrich, R., Cherubini, Y., Meggers, H., 2010. Climate and sea level induced turbidite activity in a canyon system offshore the hyperarid Western Sahara (Mauritania): the Timiris Canyon. Mar. Geol. 275, 178–198. https://doi.org/10.1016/j.margeo.2010.05.011.

Huang, C., Hinnov, L.A., 2019. Astronomically forced climate evolution in a saline lake record of the middle Eocene to Oligocene, Jianghan Basin, China. Earth Planet Sci. Lett. 528, 5–13. https://doi.org/10.1016/j.epsl.2019.115846.

Huang, C.J., 2014. The current status of cy clostratigraphy and astrochronology in the Mesozoic, 048-066 Earth Sci. Front. 21. https://doi.org/10.13745/j.esf.2014.02.005 (in Chinese).

Huang, L.Q., Liu, W., 2016. Characteristics of tempestite of lower ordovician tongzi Formation,in the longshan Area,Northwestern hunan and its geological significance. Acta Sedimentol. Sin. 34, 830–841. https://doi.org/10.14027/j.cnki.cjxb.2016.05.003 (in Chinese).

Huang, Y.T., Wen, L., Yao, G.Q., Jiang, P., 2018. Sedimentary characteristics of thick fine grained shallow marine gravity flow deposits from Huangliu Formation in Dongfang area, Yinggehai Basin,China. Acta Pet. Sin. 39, 290–303. CNKI:SUN:SYXB.0.2018-03-004(in Chinese).

He, W.J., Gan, J., Liu, F., Jiao, X.Y., Luo, W., Huang, C., 2019. Sedimentary characteristics and development of gravityflow in the upper submember of the first

memberof Liushagang Formation in Weixi'nan Sag. Pet. Geol. Recovery Effic. 26, 31–37. https://doi.org/10.13673/j.cnki.cn37-1359/te.2019.03.004 (in Chinese).
Ikeda, M., Tada, R., 2014. A 70 million year astronomical time scale for the deep-sea bedded chert sequence (Inuyama, Japan): implications for Triassic–Jurassic geochronology. Earth Planet Sci. Lett. 399, 30–43. https://doi.org/10.1016/j.epsl.2014.04.031.
Islam, T., Peterson, R.E., 2009. Climatology of landfalling tropical cyclones in Bangladesh 1877-2003. Nat. Hazards 48, 115–135. https://doi.org/10.1007/s11069-008-9252-4.
Jiang, H., 2010. Dynamical mechanism and depositional responses of turbidity current sedimentation. Oil Gas Geol. 31, 428–435. https://doi.org/10.11743/ogg20100405 (in Chinese).
Jiang, Z.X., 2010. Studies of depositional systems and sequence stratigraphy:the present and the future. Oil Gas Geol. 31, 535–541. CNKI:SUN:SYYT.0.2010-05-003(in Chinese).
Jin, J.H., Cao, Y.C., Wang, J., Yang, T., Liu, J., Wang, X.Z., Wang, S.P., 2019. New discovery of hyperpyenal flow deposits in the El1x section of the steep slope belt in the Weixinan sag. Earth Sci. Front. 26, 250–258. https://doi.org/10.13745/j.esf.sf.2019.5.16 (in Chinese).
Jiang, Z.X., 2018. Sedimentary dynamics of windfiled-source-basin system. Science Press, Beijing.
Jin, Z.H., 2017. The Study on Sedimentary Environment of Fine GrainedRocks of the Upper F ourth Member of Paleogene ShahejieF ormation, Dongying Sag. M.S. thesis, China University of Geosciences, Beijing), p. 82pp.
Jin, S.D., Liu, S.B., Li, Z., Chen, A.Q., Ma, C., 2022. Astrochronology of a middle Eocene lacustrine sequence and sedimentary noise modeling of lake-level changes in Dongying Depression, Bohai Bay Basin. Palaeogeogr. Palaeoclimatol. Palaeoecol. 585, 110740. https://doi.org/10.1016/J.PALAEO.2021.110740.
Kutzbach, J.E., Liu, X., Liu, Z., Chen, G., 2008. Simulation of the evolutionary response of global summer monsoons to orbital forcing over the past 280,000 years. Clim. Dynam. 30, 567–579. https://doi.org/10.1007/s00382-007-0308-z.
Leynaud, D., Mienert, J., Vanneste, M., 2009. Submarine mass movements on glaciated and non-glaciated European continental margins: A review of triggering mechanisms and preconditions to failure. Mar. Pet. Geol. 26, 618–632. https://doi.org/10.1016/j.marpetgeo.2008.02.008.
Li, A.Q., Hu, L., Wang, Z.Z., Li, S.Y., Li, M., 2021. Sedimentary evolution of meishan formation submarine fan in ledong sag, qiongdongnan Basin and its significance in hydrocarbon exploration. Pet. Geol. Recovery Effic. 28, 76–84. https://doi.org/10.13673/j.cnki.cn37-1359/te.2021.02.010 (in Chinese).
Li, M.S., Ogg, J., Zhang, Y., Huang, C.J., Hinnov, L., Chen, Z.Q., Zou, Z.Y., 2016. Astronomical tuning of the end-permian extinction and the early triassic epoch of south China and Germany. Earth Planet Sci. Lett. 441, 10–25. https://doi.org/10.1016/j.epsl.2016.02.017.
Li, X.D., Que, Y., Huan, Y.Q., 2019. Deep-water channel deposits of contour current in the lower part of Middle Ordovician Kelimoli Formation of Shixiagu section in Zhuozishan area, western margin of Ordos Basin. J. Palaeogeogr. 21, 321–338. https://doi.org/10.7605/gdlxb.2019.02.018 (in Chinese).
Lin, W., Jiang, Z.X., Xiang, S.A., You, G.Q., Tian, J.J., 2008. Researches on tempestites of the member 2 and member 3 of lower pemian xiashihezi fomation in daniudi gasfield ordos basin. J. Palaeogeogr. 10, 167–174. https://doi.org/10.7605/gdlxb.2008.02.006 (in Chinese).
Liu, J.L., Liu, K.Y., 2020. Estimating stratal completeness of carbonate deposition via process-based stratigraphic forward modeling. Sci. China Earth Sci. 51, 150–158. https://doi.org/10.1360/N072020-0100 (in Chinese).
Liu, B.J., Zhang, J.Q., Xu, X.S., 1986. On the calcareous tempestites in the Lower Permian of Silong, Xingwen, Sichuan. Acta Geol. Sin. 60, 55-67-121-122, (in Chinese).
Luan, X.W., Kong, X.X., Zhang, J.L., Jiang, L., Peng, Y.X., Cai, Y., 2022. Astronomical forcing of origins of eocene carbonate-bearing fine-grained sedimentary rock in dongying sag. Acta Sedimentol. Sin. (in Chinese) https://kns.cnki.net/kcms/detail/62.1038.p.20220810.1624.002.html.
Lv, A.M., 2017. Review of researches on cyclonic storms over the Bay of Bengal. J. Mar. Meteor. 37, 13–21. https://doi.org/10.19513/j.cnki.issn2096-3599.2017.02.002 (in Chinese).
Macquaker, J., Bentley, S.J., Bohacs, K.M., 2010. Wave-enhanced sediment-gravity flows and mud dispersal across continental shelves: reappraising sediment transport processes operating in ancient mudstone successions. Geology 38, 947–950. https://doi.org/10.1130/G31093.1.
Ma, C., Meyers, S.R., Sageman, B., 2019. Testing Late Cretaceous astronomical solutions in a 15 million year astrochronologic record from North America. Earth Planet Sci. Lett. 513, 1–11. https://doi.org/10.1016/j.epsl.2019.01.053.
Ma, S., Chen, S.Y., Wang, F., Shao, P.C., Wang, Z.J., 2017. Sedimentary characteristics and geological significance of storm deposite of paleozoic in the olongbluk block. Acta Sedimentol. Sin. 35, 35–45. https://doi.org/10.14027/j.cnki.cjxb.2017.01.004 (in Chinese).
Mei, M.X., 2015. Conceptual change from depositional sequences to eustatic sequences: an important de-velopment in sequence stratigraphy. J. Stratigr. 39, 58–73. https://doi.org/10.19839/j.cnki.dcxzz.2015.01.006 (in Chinese).
Mulder, T., Savoye, B., Syvitski, J., Parize, O., 1997. Des courants de turbidité hyperpycnaux dans la tête du canyon du Var? Données hydrologiques et observations de terrain. Oceanol. Acta 20, 110–154. https://archimer.ifremer.fr/doc/00093/20421.
Mulder, T., Syvitski, J.P., 1995. Turbidity currents generated at river mouths during exceptional discharges to the world oceans. J. Geol. 103, 285–299. https://doi.org/10.1086/629747.
Mulder, T., Syvitski, J.P., Migeon, S., Faugeresa, J.C., Savoye, B., 2003. Marine hyperpycnal flows:Initiati-on, behavior and related deposits. A review. Mar. Pet. Geol. 20, 861–882. https://doi.org/10.1016/j.marpe-tgeo.2003.01.003.
Musgrave, K.D., Davis, C.A., Montgomery, M.T., 2008. Numerical simulations of the formation of hurricane gabrielle (2001). Mon. Weather Rev. 136, 3151–3167. https://doi.org/10.1175/2007MWR2110.1.
Pang, X., 2012. Sequence stratigraphy configuration of deepwatergravity-flow sediments and its controls: a line ofthinking in sequence stratigraphy of gravity-flowsediments in Baiyun deepwater area, the northe-rn South China Sea. China Offshore Oil Gas 24, 1–8. https://doi.org/10.3969/j.issn.1673-1506.2012.02.001 (in Chinese).
Peng, J., Xu, T.Y., Yu, L.D., 2020. Characteristics and controlling factors of lacustrine fine-grained Sediments of the fourth member of Shahejie Formation in Dongying Sag. Lithol. Reservoirs 32, 1–12. https://doi.org/10.12108/yxyqc.20200501 (in Chinese).
Peng, J., Yu, L.D., Xu, T.Y., Han, H.D., Yang, Y.M., Zeng, Y., Wang, Y.B., 2022. Logging identification of milankovitch cycle and environmental response characteristics of lacustrine shale—a case study on Es4scs in well Fanye 1 , Dongying Sag , Jiyang Depression , Bohai Bay Basin. Oil Gas Geol. 4, 957–969. https://doi.org/10.11743/ogg20220417 (in Chinese).
Petter, A.L., Steel, R.J., 2006. Hyperpycnal flow variability and slope or ganization on an Eocene shelf margin, Central Basin, Spitsbergen. AAPG Bull. 90, 1451–1472. https://doi.org/10.1306/04240605144.
Pierau, R., Hanebuth, T., Krastel, S., Henrich, R., 2010. Late quaternary climatic events and sea-level cha-nges recorded by turbidite activity, dakar canyon, nw africa. Quat. Res. (Tokyo) 73, 385–392. https://doi.org/10.1016/j.yqres.2009.07.010.
Pietras, J.T., Carroll, A.R., Rhodes, M.K., 2003. Lake basin response to tectonic-drainage diversion: eocene green river formation, Wyoming. J. Paleolimnol. 30, 115–125. https://doi.org/10.1023/A:1025518015341.
Plint, A.G., 2014. Mud dispersal across a Cretaceous prodelta: stormgenerated, wave-enhanced sediment gravity flows inferred from mudstone microtexture and microfacies. Sedimentology 61, 609–647. https://doi.org/10.1111/sed.12068.
Potter, P.E., Maynard, J.B., Depetris, P.J., 2005. Mud and Mudstones. Springer Press, Berlin, pp. 1–3.
Quan, C., Liu, Y.S., Utescher, T., 2012. Paleogene temperature gradient, seasonal variation and climate evo-lution of northeast China. Palaeogeogr. Palaeoclimatol. Palaeoecol. 313, 150–161. https://doi.org/10.1016/j.palaeo.2011.10.016.
Quan, C., Liu, Z., Utescher, T., Jin, J., Shu, J., Li, Y., Liu, Y.S., 2014. Revisiting the Paleogene climate pattern of East Asia: a synthetic review. Earth Sci. Rev. 139, 213–230. https://doi.org/10.1016/j.earscirev.2014.09.005.
Renaut, R.W., Gierlowski-Kordesch, E.H., 2010. Lakes. Facies Models 4. Geological Association of Canada, Newfoundland, pp. 541–571, 9781897095508.
Ruhl, M., Hesselbo, S.P., Hinnov, L.A., Jenkyns, H.C., Xu, W., Riding, J.B., Storm, M., Minisini, D., Ullmann, C.V., Leng, M.J., 2016. Astronomical constraints on the duration of the Early Jurassic Pliensbachian Stage and global climatic fluctuations. Earth Planet Sci. Lett. 455, 149–165. https://doi.org/10.1016/j.epsl.2016.08.038.
Schieber, J., Southard, J., Thaisen, K., 2007. Accretion of mudstone beds from migrating floccule ripples. Science 318, 1760–1763. https://doi.org/10.1126/science.1147001.
Shao, L.Y., Xu, X.T., Wang, S., Wang, D.D., Gao, D., Wang, X.T., Lu, J., 2021. Research progress of pal-aeogeography and palaeoenvironmental evolution of coal-bearing series in China. J. Palaeogeogr. 23, 19–38. https://doi.org/10.7605/gdlxb.2021.01.002 (in Chinese).
Shi, J.Y., Jin, J.Y., Liu, Q.Y., Huang, Z.K., Zhang, R., 2019a. Quantitative classification of high-frequency sequences in fine-grained lacustrine sedimentary rocks based on Milankovitch theory. Oil Gas Geol. 40, 1205–1214. CNKI:SUN:SYYT.0.2019-06-005(in Chinese).
Shi, J.Y., Jin, J.Y., Liu, Q.Y., Zhang, R., Huang, Z.K., 2019b. Cyclostratigraphy and astronomical tuning of the middle eocene terrestrial successions in the Bohai Bay Basin, Eastern China. Global Planet. Change 174, 115–126. https://doi.org/10.1016/j.gloplacha.2019.01.001.
Shi, J.Y., Jin, J.Y., Liu, Q.Y., Huang, Z.K., 2020. Depositional process and astronomical forcing model of lacustrine finegrained sedimentary rocks: a case study of the early Paleogene in the Dongying Sag, Bohai Bay Basin. Mar. Petrol. Geol. 113, 1–10. https://doi.org/10.1016/j.marpetgeo.2019.08.023.
Sierro, F.J., Ledesma, S., Flores, José-Abel, Torrescusa, S., Martínez del, O., Wenceslao, 2000. Sonic and g-amma-ray astrochronology: cycle to cycle calibration of atlantic climatic records to mediterranean sapr-opels and astronomical oscillations. Geology 28, 695–698. https://doi.org/10.1130/0091-7613(2000)28<695:SAGACT>2.0.CO, 2.
Sun, S.Y., Liu, H.M., Cao, Y.C., Zhang, S., Wang, Y., Yang, W.Q., 2017. Milankovitch cycle of lacustrine deepwater fine-grained sedimentary rocks and its significance to shale oil: a case study of the upper Es4 member of well NY1 in Dongying sag. J. China Univ. Min. Technol. 46, 846–858. https://doi.org/10.13247/j.cnki.jcumt.000638 (in Chinese).
Tan, M.X., Zhu, X.M., Zhu, S.F., 2015. Research on sedimentary process and characteristics of hyperpyc-nal flows. Geol. J. China Univ. 21, 94–104. https://doi.org/10.16108/j.issn1006-7493.2014095 (in Chinese).
Tan, X.F., Jiang, Y.X., Li, J., Xue, W.W., Li, Z.M., 2015. Sedimentary record and origin of high frequency cycles in the Paleogene kongdian Formation in the Jiyang depression. Oil Gas Geol. 1, 61–72. https://doi.org/10.11743/ogg20150108 (in Chinese).
Tyson, R., 2001. Sedimentation rate, dilution, preservation and total organic carbon:

some results of a modelling study. Org. Geochem. 32, 333–339. https://doi.org/10.1016/S0146-6380(00)00161-3.
Urlaub, M., Talling, P.J., Masson, D.G., 2013. Timing and frequency of large submarine landslides: implications for understanding triggers and future geohazard. Quat. Sci. Rev. 72, 63–82. https://doi.org/10.1016/j.quascirev.2013.04.020.
Valero, L., Garcés, M., Cabrera, L., Costa, E., Sáez, A., 2014. 20myr of eccentricity paced lacustrine cycle-s in the Cenozoic Ebro Basin. Earth Planet Sci. Lett. 408, 183–193. https://doi.org/10.1016/j.epsl.2014.10.007.
Wang, D.P., 1991. The sedimentation and formation machanism of lacustrine endogenic debris flow. Acta Geol. Sin. 4, 299–318 doi:CNKI:SUN:DZXE.0.1991-04-000 (in Chinese).
Wang, B., Ding, Q.H., 2008. Global monsoon: dominant mode of annual variation in the tropics. Dynam. Atmos. Oceans 44, 165–183. https://doi.org/10.1016/j.dynatmoce.2007.05.002.
Wang, L., Khalid, L., Muhammad, R., Liu, X.H., 2018. The Genesis , Classification , Problems and Prospects of Microbial Carbonates: Implications from the Cambrian Carbonate of North China Platform. Adv. Earth Sci. 33, 1005–1023. https://doi.org/10.11867/j.issn.1001-8166.2018.10.1005 (in Chinese).
Wang, D., Lu, S., Han, S., Sun, X., Quan, C., 2013. Eocene prevalence of monsoon-like climate over eas-tern China reflflected by hydrological dynamics. Journal of Asian Earth Sci.s 62, 776–787. https://doi.org/10.1016/j.jseaes.2012.11.032.
Van Loon, H., 1990. Climates of the oceans. China ocean press, Beijing, 7-5027-0000-9 (in Chinese).
Wang, J., Jiang, Z., Zhang, Y., 2015a. Subsurface lacustrine storm-seiche depositional model in the eocene l-ijin sag of the bohai bay basin, east China. Sediment. Geol. 328, 55–72. https://doi.org/10.1016/j.sedgeo.2015.07.014.
Wang, D.W., Wu, S.G., Wang, Y.M., Yao, G.S., Qin, Z.L., 2015b. Deep-water sediment cycles in the qiongdongnan basin. Chin. Sci. Bull. 60, 933–943. https://doi.org/10.1360/N972014-00477.
Wang, Y.J., Zhao, D.F., Lu, Q.R., Zhang, Y.Y., Liu, J., Guo, Y.H., 2020. Impact of laminae and interlaye-r sedimentary structure on the storage and brittleness of shale reservoirs-taking longmaxi formatio-n shale in Sichuan Basin as an example. Unconventional Oil & Gas 7, 33–40. https://doi.org/10.3969/j.issn.2095-8471.2020.06.006 (in Chinese).
Wei, X.J., Jiang, Z.X., Li, Y.F., Zhang, Y.F., Zhao, B.Y., Wang, J.H., 2014. Sedimentary characteristics and controlling factors of lacustrinestorm deposits of the Paleogene Shahejie Formation in lijin sag, dongying sag, bohai Bay Basin. J. Palaeogeogr. 16, 377–384. CNKI:SUN:GDLX.0.2014-03-008(in Chinese).
Wilson, R.D., Schieber, J., 2014. Muddy prodeltaic hyperpycnites in the LowerGenesee group of central New York, USA: implications for mudtransport in epicontinental seas. J. Sediment. Res. 84, 866–874. https://doi.org/10.2110/jsr.2014.70.
Wu, H.C., Zhang, S.H., Feng, Q.L., Fang, N.Q., Yang, T.S., Li, H.Y., 2011. Theoretical Basis,Research Advancement and Prospects of Cyclostratigraphy. Earth Sci. (Wuhan, China) 36, 409–428, doi:10.3799/dqkx.2011.045. (in Chinese)
Wu, J., Jiang, Z.X., Liang, C., 2017. Lithofacies characteristics of fine grained sedimentary rocks in the upper submember of Member 4 of Shahejie Formation, Dongying sag and their relationship. Acta Pet. Sin. 38, 1110–1122. https://doi.org/10.7623/syxb201710002 (in Chinese).
Wu, J., Jiang, Z.X., Wang, X., 2018. Sequence stratigraphy characteristics of lacustrine fine grained sedimentary rocks :A case study of the upper fourth member of Paleogene Shahejie Formation, Dongying Sag,Bohai Bay Basin. Nat. Gas Geosci. 29, 199–210. CNKI:SUN:TDKX.0.2018-02-006(in Chinese).
Xing, Z.C., Zhang, Z.T., Lin, C.S., Zhang, B., Hong, F.H., Gong, Y., 2020. Sedimentary types and features of gravity flow depositional systems from late oligocene to early Miocene in liwan sag, Pearl River Mouth basin. J. Palaeogeogr. 22, 1143–1156. https://doi.org/10.7605/gdlxb.2020.06.077 (in Chinese).
Xu, J.P., 2013. Accomplishments and challenges in measuring turbidity currents in submarine canyons. Adv. Earth Sci. 28, 552–558. https://doi.org/10.11867/j.issn.1001-8166.2013.05.0552 (in Chinese).
Xu, J.P., 2014. Turbidity current research in the past century: an overview. Period. Ocean Univ. China 44, 98–105. https://doi.org/10.16441/j.cnki.hdxb.2014.10.014 (in Chinese).
Yang, R.C., Jin, Z.Z., Sun, D.S., Fan, A.P., 2015. Discovery of hyperpycnal flow deposits in the late triassic lacustrine ordos basin. Acta Sedimentol. Sin. 33, 10–20. https://doi.org/10.14027/j.cnki.cjxb.2015.01.002 (in Chinese).
Yang, R.C., Tian, Y., 2020. Discussion on the scientific issues in frontiers of A stronomical cycles and hyperpycnal flow deposits. Unconventional Oil & Gas 7, 1–7. https://doi.org/10.3969/j.issn.2095-8471.2020.05.001 (in Chinese).
Yan, H.M., Wang, L., Yang, Y., Yang, K.L., Jin, Y., Liu, J., 2020. Relationship between storm activity and summer monsoon onset in Bay of Bengal Basin and their precursor signals. J. Trop. Meteorol. 36, 145–146. https://doi.org/10.16032/j.issn.1004-4965.2020.015.
Yang, T., Cao, Y.C., Wang, Y.Z., Zhang, S.M., Zhang, H.M., Wang, S.J., 2015. Sediment Dynamics Process and Sedimentary Characteristics of Hyperpycnal Flows. Geol. Rev. 61, 23–33. https://doi.org/10.16509/j.georeview.2015.01.006 (in Chinese).
Yang, T., Cao, Y.C., Wang, Y.Z., Zhao, S.M., 2015. Types, sedimentary characteristics and genetic mechanisms of deep water gravity flows:a case study of the middle submember in Member 3 of Shahejie Formation in Jiyang depression. Acta Pet. Sin. 36, 1048–1059. https://doi.org/10.7623/syxb201509003 (in Chinese).
Yang, X., Liu, B., Zhang, J.C., Huo, Z.P., 2019. Identification of sedimentary responses to the milankovi-tch cycles in the K2qn1 formation, gulong depression. Acta Sedimentol. Sin. 37, 661–673. https://doi.org/10.14027/j.issn.1000-0550.2018.178 (in Chinese).
Yu, L.D., Peng, J., Xu, T.Y., Wang, Y.B., Han, H.D., 2021. A study on astronomical cycle identification and environmental response characteristics of lacustrine deep-water fine-grained sedimentary rocks : A case study of the lower submember of member 3 of Shahejie Formation in well Fanye 1 of dongying Sag,Bohai Bay Basin,China. Geofluids. https://doi.org/10.1155/2021/5595829.
Yuan, J., Liang, H.Y., Liang, B., Dong, D.T., Min, W., Song, P., Li, H.Y., 2016. Sedimentary characteristics and development model of lacustrine gravity flow: a case studyof Dainan Formation in deep sag belt of Gaoyou depression , Northern Jiangsu Basin. Acta Pet. Sin. 37, 348–359. https://doi.org/10.7623/syxb201603007 (in Chinese).
Yuan, X.J., Lin, S.H., Liu, Q., Yao, J.L., Wang, L., Guo, H., Deng, X.Q., Cheng, D.W., 2015. Lacustrine fine-grained sedimentary features and organic-rich shale distribution pattern: a case study of Chang 7 Member of Triassic Yanchang Formation in Ordos Basin, NW China. Petrol. Explor. Dev. 42, 34–43, 10.11698/PED.2015.01.04(in Chinese).
Zeng, D.Y., Shi, Z.Q., Zhang, H., An, H.Y., Zhang, H.J., 2011. Tempestite of early triassic feixianguan Formation in shangsi section, guanyuan:are they extreme climatic event under megamonsoon system? Acta Sedimentol. Sin. 29, 440–448. https://doi.org/10.14027/j.cnki.cjxb.2011.03.015 (in Chinese).
Zhao, C., Liu, S.G., Song, J.M., Tang, X., Lai, D., 2019. Sedimentary characteristics and geological significance of tempestites in the fourth member of the leikoupo formation at the hanwang section, western Sichuan Basin. Acta Sedimentol. Sin. 37, 94–103. https://doi.org/10.14027/j.issn.1000-0550.2018.140 (in Chinese).
Zhao, W.Z., Wang, X., Hu, S., Zhang, S., Wang, H., Guan, S., Ye, Y., Ren, R., Wang, T., 2019. Hydrocarbon generation characteristics and exploration prospects of Proterozoic source rocks in China. Sci. China Earth Sci. 62, 909–934. https://doi.org/10.1007/s11430-018-9312-4.
Zhang, S.M., Cao, Y.C., Zhu, R.K., Wang, W., Tu, J.Q., Mao, Z.G., Bai, B., 2016. The lithofacies and depositional environment of fine grained sedimentary rocks of Xiaohu Subsag in Y abulai Basin. Nat. Gas Geosci. 27, 309–319. https://doi.org/10.11764/j.issn.1672-1926.2016.02.0309 (in Chinese).
Zhang, J.G., Jiang, Z.X., Liang, C., Wu, J., Xian, B., Li, Q., 2016. Lacustrine massive mudrock in the Eocene Jiyang Depression, Bohai Bay Basin, China: Nature, origin and significance. Mar. Pet. Geol. 77, 1042–1055. https://doi.org/10.1016/j.marpetgeo.2016.08.008.
Zhang, H., Li, F.J., Shen, F., Chen, Z.A., Ni, Z.Y., 2019. Storm deposits characteristics and its geological significance in the devonian yangmaba formation from shigouli section, longmenshan area, Sichuan Basin. J. Palaeogeogr. 21, 441–450. https://doi.org/10.7605/gdlxb.2019.03.027 (in Chinese).
Zhang, X., Zhang, J.L., 2009. Composite deposits of beach bar and tempestite in the upper fourth me-mber of Shahejie Formation in the central Uplift belt of Huimin depression. Acta Sedimentol. Sin. 27, 246–253. CNKI:SUN:CJXB.0.2009-02-007(in Chinese).
Zhang, Y.D., Jiang, Z.X., Du, K.F., Zhang, J.G., Nian, T., Zhou, X.W., Luo, D.T., Wang, L., 2019. Sedimentary characteristics and significances of storm deposition in chang-8 oil layer of triassic yanchang formation, zhidan fuxian area, ordos basin. Acta Pet. Sin. 40, 813–822. https://doi.org/10.7623/syxb201907005 (in Chinese).
Zhao, X.Z., Zhou, L.H., Pu, X.G., Jin, F.M., Shi, Z.N., Xiao, D.Q., Han, W.Z., Jiang, W.Y., Zhang, W., Wang, H., 2019. Favorable formation conditions and enrichment characteristics of lacustrine facies shaleoil in faulted lake basin :a case study of Member 2 of Kongdian Formation inCangdong sag , Bohai Bay Basin. Acta Pet. Sin. 40, 1013–1029. CNKI:SUN:SYXB.0.2019-09-001(in Chinese).
Zheng, N., Jiang, Z.X., Li, T.D., Geng, S.F., You, G.Q., He, Y.B., 2010. Basic characteristics of tempestite sediments of Middle Sha 3 Formation in Gunan Subsag of Bohai Bay Basin and their geological significance. Geol. China 37, 1191–1198. https://doi.org/10.3969/j.issn.1000-3657.2010.04.033 (in Chinese).
Zheng, B.S., Mou, C.L., Liang, W., Chen, C., Xu, P.H., Sun, X.Y., 2016. Discovery and significance of the storm deposit within the lower cambrian qingxudong Formation in the dingtai area, northwestern guizhou. Acta Sedimentol. Sin. 34, 478–486. https://doi.org/10.14027/j.cnki.cjxb.2016.03.005 (in Chinese).
Zhou, J.H., Xian, B.Z., Zhang, J.G., Zhong, Q., Chen, P., 2022. Organic matter enrichment law of lacustri-ne shale constrained by high resolution cyclostratigraphy: a case study from the lower sub-member of Member 3 of Paleogene Shahejie Formation,Dongying sag. J. Palaeogeogr. 4, 759–770. https://doi.org/10.7605/gdlxb . 2022 . 04 . 058 (in Chinese).
Zhou, L.H., Sun, Z.H., Tang, G., Xiao, D.Q., Cai, Z., Wang, H.Q., Su, J.Q., Huan, S.J., Ge, W., Chen, C.W., 2020. Pliocene hyperpycnal flow and its sedimentary pattern in D block of Rakhine Basin in Bay of Bengal. Petrol. Explor. Dev. 47, 297–308. https://doi.org/10.1016/S1876-3804(20)60049-0 (in Chinese).
Zhong, J.H., Song, G.X., Ni, L.T., Sun, N.L., Hao, B., Ge, Y.Z., Xue, C.Q., Sun, J.Y., Liu, C., Cao, M.C., 2019. Modern non-seismically induced deformation bedding in the lower reaches of the yellow river delta. Acta Sedimentol. Sin. 37, 239–253. https://doi.org/10.14027/j.issn.1000-0550.2018.168 (in Chinese).
Zhong, J.H., Ni, L.T., Sun, N.L., Hao, B., Xue, C.Q., Shao, Z.F., Mao, C., Song, G.X., Ge, Y.Z., Chen, B., Liu, S.X., Cao, M.C., Liu, C., Peng, C.F., Gu, D.H., Wang, C.N., Wang, Y.Q., Li, C., 2020. Lacustrine storm and tempestite of Lower Cretaceous in the Lingshan island, Qingdao, Shandong. Acta Geol. Sin. 94, 3036–3061. doi:10.19762/j.cnki.dizhixuebao.2020040. (in Chinese).
Zhong, J.H., Ning, L.T., Sun, N.L., Hao, B., Xue, C.Q., 2021. Discovery and significance of lake storm deposits in the triassic-jurassic of eastern dongsheng, ordos basin. Acta Sedimentol. Sin. 39, 353–373. https://doi.org/10.14027/j.issn.1000-0550.2020.030 (in Chinese).